

University of Nevada, Reno

**Effects of Controlling Parameters and Their Spatial Variability on  
Heat Flow in the Vadose Zone**

A thesis submitted in partial fulfillment of the  
requirements for the degree of Master of Science in  
Hydrogeology

By

Nicholas Paasche

Dr. Clay Cooper/Thesis Advisor

May, 2016

© Copyright by Nicholas Paasche, 2016.

All Rights Reserved



THE GRADUATE SCHOOL

We recommend that the thesis prepared under our  
supervision by

**NICHOLAS PAASCHE**

Entitled

**Effects of Controlling Parameters and Their Spatial  
Variability on  
Subsurface Heat Flow**

be accepted in partial fulfillment of the requirements for  
the degree of

MASTER OF SCIENCE

Clay Cooper, Ph.D., Advisor

Wendy Calvin, Ph.D., Committee Member

Paul Verburg, Ph.D., Graduate School Representative

David W. Zeh, Ph.D., Dean, Graduate School

May, 2016

## ABSTRACT

While the use of geothermal energy is becoming more common, a key factor holding back the growth of geothermal energy production is the cost of exploration. Rapid shallow (two meter) temperature measurement is a relatively inexpensive exploration method that can be used to locate blind geothermal systems. This method has been successfully used to locate geothermal anomalies at two meters depth that are representative of a similar geothermal pattern at a greater depth (Coolbaugh et al., 2007). However, studies have shown that increased temperatures at two meters depth are not always analogous to increased temperature at a deeper depth (Olmsted and Ingebritsen, 1986). Therefore, a better understanding of the parameters that control heat flow to shallow depths is needed.

This study uses numerical modeling to assess the effect of material heterogeneities on heat transport in the vadose zone. The TOUGH2 computer program is used to numerically simulate heat, water, and air transport through two-dimensional porous media. A 100 by 100 meter grid was created with a water table at the lower boundary held constant at 95°C and the average surface temperature at the upper boundary held constant at 20°C. Intrinsic permeability, porosity, residual liquid saturation and thermal conductivity of the porous media were systematically altered in different spatial patterns to determine the controlling factors affecting heat flow in the vadose zone. Results of this study indicate that individual changes in the parameters tested do not result in significant horizontal changes in temperature at shallow depths. Although these individual changes in the parameters tested are not enough to significantly change

temperature horizontally at two meters depth, the results reveal conditions under which heat flows more readily to the surface.

## ACKNOWLEDGMENTS

I am grateful to the many people who have made this thesis possible and because of whom my time at the University of Nevada, Reno has been a life changing experience that I will value forever.

First and foremost among those people is my advisor, Clay Cooper. His guidance, insight and most of all patience proved invaluable in my quest to master the research necessary to write this thesis. I could not have asked for a more dedicated mentor during this process. Besides my advisor, I would like to thank the rest of my thesis committee: Dr. Paul Verburg and Dr. Wendy Calvin, for their support and encouragement.

Funding for this project was provided by the Geology Department through the US Department of Energy. Additional funding was provided in the form of a scholarship from the Nevada Petroleum and Geothermal Society. I cannot say enough about the generosity of the sponsors of this project and how this research would not have been possible without this funding. My sincere thanks also goes to the Desert Research Institute for providing me an opportunity to work in a real world environment with state of the art resources, and who gave me unfettered access to the research facilities. Without that precious support it would not have been possible to conduct this research.

I thank my colleagues, in particular Susie Rybarski, for the time she selflessly gave encouraging me, discussing my research, and editing my thesis. Last but not the least, I would like to thank my family for their unwavering faith in me and for supporting me throughout my time at UNR and while writing this thesis.

**TABLE OF CONTENTS**

ABSTRACT .....	i
ACKNOWLEDGMENTS .....	iii
LIST OF FIGURES .....	v
LIST OF TABLES .....	v
INTRODUCTION .....	1
1.1 Background .....	1
1.2 General Geothermal Concepts .....	5
1.3 Related Work.....	7
1.4 Purpose/Objective .....	11
METHODS .....	16
2.1 TOUGH2.....	16
2.2 Model Domain and Boundary Conditions .....	17
2.3 Modeling Methods and Initial Conditions .....	21
RESULTS .....	25
3.1 Permeability Results.....	25
3.2 Thermal Conductivity Results.....	36
3.3 Porosity Results.....	42
3.4 Residual Liquid Saturation Results .....	47
3.5 Additional Modeling Results .....	53
DISCUSSION .....	57
4.1 Comparisons of Parameters Tested.....	57
4.2 Comparison to Related Work.....	60
4.3 Modeling Limitations and Realistic Expectations .....	61
4.4 Future Work .....	62
CONCLUSION.....	64
5.1 General Conclusions .....	64
REFERENCES .....	66
APPENDIX.....	68

**LIST OF TABLES**

Table 1: Modeling scenarios and how the parameters alter from the base model.....	22
Table 2: Approximate changes in temperature (°C) at two meters depth for all 25 initial simulations.....	57
Table 3: Approximate changes in temperature (°C) throughout the entire model for all 25 initial simulations.....	58



## LIST OF FIGURES

Figure 1: Comparison of CO <sub>2</sub> emissions from electricity generation by geothermal, natural gas, oil, and coal in the US in 2003. ....	2
Figure 2: Comparison of two-meter temperature measurements to temperature at 30 meters depth at Desert Queen area. White dots represent 12 gradient wells and the black lines represent temperature contours at a depth of 30 meters with 18°C separation. The colored dots represent the two-meter temperature measurements; dark blue = <23°C, light blue = 23—24°C, green = 24—25°C, yellow = 25—27°C, orange = 27—30°C, red = 30—33°C. Image is from Coolbaugh et al., 2007. ....	10
Figure 3: Conceptual image of an isolated geothermal anomaly in homogenous material. ....	12
Figure 4: Conceptual image of an isolated geothermal anomaly in heterogeneous material. ....	13
Figure 5: Conceptual image of a geothermal anomaly with uniform temperature at the lower boundary in heterogeneous material. ....	14
Figure 6: Homogeneous 2D model diagram showing model dimensions, initial boundary temperatures and conductive heat flow.....	19
Figure 7: Heterogeneous patterns in which the parameters tested are altered.....	20
Figure 8: Results of the permeability simulations in a homogeneous model domain. Colored temperature contours are shown in °C and are overlain by heat flow vectors. a) Simulation 2 - Low permeability (10 <sup>-12</sup> m <sup>2</sup> ) with heat flow up to 2 J/s; b) Simulation 3 - High permeability (10 <sup>-10</sup> m <sup>2</sup> ) with heat flow up to 741 J/s.....	26
Figure 9: Results of the permeability simulations in a large checkerboard model domain. Colored temperature contours are shown in °C and are overlain by heat flow vectors. a) Simulation 10 - Low permeability (10 <sup>-12</sup> m <sup>2</sup> ) with heat flow up to 2 J/s; b) Simulation 11 - High permeability (10 <sup>-10</sup> m <sup>2</sup> ) with heat flow up to 504 J/s.....	27
Figure 10: Results of the permeability simulations in a vertical layers model domain. Colored temperature contours are shown in °C and are overlain by heat flow vectors. a) Simulation 18 - Low permeability (10 <sup>-12</sup> m <sup>2</sup> ) with heat flow up to 2 J/s; b) Simulation 19 - High permeability (10 <sup>-10</sup> m <sup>2</sup> ) with heat flow up to 494 J/s.....	28
Figure 11: Heat flow vectors overlaying a liquid saturation plot for a large checkerboard model with high permeability (Simulation 11) next to the large checkerboard model pattern. This is the same model as 9b, showing liquid saturation instead of temperature.	30
Figure 12: Temperature plot of the large checkerboard model with high permeability (10 <sup>-10</sup> m <sup>2</sup> ) (Simulation 11) on the left and low permeability (10 <sup>-12</sup> m <sup>2</sup> ) (Simulation 10) on the right overlain by liquid velocity vectors. Temperature is in °C.....	31
Figure 13: Temperature plot of the large checkerboard model with altered high permeability (10 <sup>-10</sup> m <sup>2</sup> ) (Simulation 11) on the left and altered low permeability (10 <sup>-12</sup> m <sup>2</sup> ) (Simulation 10) on the right overlain by gas velocity vectors. Temperature is in °C.....	32

Figure 14: Temperature profile in the center (column 13) of the high and low homogeneous permeability models.....	35
Figure 15: Results of the thermal conductivity simulations in a homogeneous model domain. Colored temperature contours are shown in °C and are overlain by heat flow vectors. a) Simulation 4 - Low thermal conductivity ( $0.5 \text{ Wm}^{-1}\text{K}^{-1}$ ) with heat flow up to 95 J/s; b) Simulation 5 - High thermal conductivity ( $3.5 \text{ Wm}^{-1}\text{K}^{-1}$ ) with heat flow up to 141 J/s. ....	38
Figure 16: Results of the thermal conductivity simulations in a large checkerboard model domain. Colored temperature contours are shown in °C and are overlain by heat flow vectors. a) Simulation 12 - Low thermal conductivity ( $0.5 \text{ Wm}^{-1}\text{K}^{-1}$ ) with heat flow up to 117 J/s; b) Simulation 13 - High thermal conductivity ( $3.5 \text{ Wm}^{-1}\text{K}^{-1}$ ) with heat flow up to 151 J/s. ....	39
Figure 17: Results of the thermal conductivity simulations in a vertical layers model domain. Colored temperature contours are shown in °C and are overlain by heat flow vectors. a) Simulation 20 - Low thermal conductivity ( $0.5 \text{ Wm}^{-1}\text{K}^{-1}$ ) with heat flow up to 130 J/s; b) Simulation 21 - High thermal conductivity ( $3.5 \text{ Wm}^{-1}\text{K}^{-1}$ ) with heat flow up to 144 J/s. ....	40
Figure 18: Results of the porosity simulations in a homogeneous model domain. Colored temperature contours are shown in °C and are overlain by heat flow vectors. a) Simulation 6 - Low porosity (0.25) with heat flow up to 134 J/s; b) Simulation 7 - High porosity (0.50) with heat flow up to 134 J/s. ....	43
Figure 19: Results of the porosity simulations in a large checkerboard model domain. Colored temperature contours are shown in °C and are overlain by heat flow vectors. a) Simulation 14 - Low porosity (0.25) with heat flow up to 150 J/s; b) Simulation 15 - High porosity (0.50) with heat flow up to 134 J/s. ....	44
Figure 20: Results of the porosity simulations in a vertical layers model domain. Colored temperature contours are shown in °C and are overlain by heat flow vectors. a) Simulation 22 - Low porosity (0.25) with heat flow up to 134 J/s; b) Simulation 23 - High porosity (0.50) with heat flow up to 134 J/s. ....	45
Figure 21: Temperature and heat flow comparison of homogeneous base model (Simulation 1) to the homogeneous, low porosity model (Simulation 6).....	46
Figure 22: Results of the residual liquid saturation simulations in a homogeneous model domain. Colored temperature contours are shown in °C and are overlain by heat flow vectors. a) Simulation 8 - Moderate residual liquid saturation (0.10) with heat flow up to 104 J/s; b) Simulation 9 - High residual liquid saturation (0.15) with heat flow up to 2 J/s. ....	48
Figure 23: Results of the residual liquid saturation simulations in a large checkerboard model domain. Colored temperature contours are shown in °C and are overlain by heat flow vectors. a) Simulation 16 - Moderate residual liquid saturation (0.10) with heat flow up to 132 J/s; b) Simulation 17 - High residual liquid saturation (0.50) with heat flow up to 121 J/s. ....	49

- Figure 24: Results of the residual liquid saturation simulations in a vertical layers model domain. Colored temperature contours are shown in °C and are overlain by heat flow vectors. a) Simulation 24 - Moderate residual liquid saturation (0.10) with heat flow up to 111 J/s; b) Simulation 25 - High residual liquid saturation (0.50) with heat flow up to 116 J/s. .... 50
- Figure 25: Heat flow vectors overlaying a liquid saturation plot for the homogeneous model with high residual liquid saturation (Simulation 9) in comparison to the base model (Simulation 1). .... 52
- Figure 26: Results of the thermal conductivity simulations with an isolated increased temperature in a large checkerboard model domain. Colored temperature contours are shown in °C and are overlain by heat flow vectors. a) Simulation 26 - Low thermal conductivity ( $0.5 \text{ Wm}^{-1}\text{K}^{-1}$ ) with heat flow up to 111 J/s; b) Simulation 27 - High thermal conductivity ( $3.5 \text{ Wm}^{-1}\text{K}^{-1}$ ) with heat flow up to 213 J/s. .... 54
- Figure 27: Results of the thermal conductivity simulations with an isolated increased temperature in a large checkerboard model domain. Colored temperature contours are shown in °C and are overlain by heat flow vectors. a) Simulation 26 - Low thermal conductivity ( $0.5 \text{ Wm}^{-1}\text{K}^{-1}$ ) with heat flow up to 111 J/s; b) Simulation 27 - High thermal conductivity ( $3.5 \text{ Wm}^{-1}\text{K}^{-1}$ ) with heat flow up to 213 J/s. .... 56

## CHAPTER 1

### INTRODUCTION

#### 1.1 Background

The world's demand for energy is increasing, and the supply of energy resources such as petroleum, natural gas, and coal is finite. The majority of global energy is produced by nonrenewable resources. As nonrenewable resources become diminished, the price of these resources will increase. Many countries are looking to produce cheaper, cleaner energy with lower CO<sub>2</sub> emissions, and geothermal energy is one way to achieve this goal. Geothermal power plants produce significantly lower CO<sub>2</sub> emissions than natural gas, oil, and coal, because in most cases the gas remains dissolved in the liquid phase as it is re-injected into the reservoir (Dickson and Faneli, 2013). The amount of CO<sub>2</sub> emissions produced by geothermal, natural gas, oil, and coal power plants in the US is illustrated in Figure 1 (Bloomfield et al., 2003).

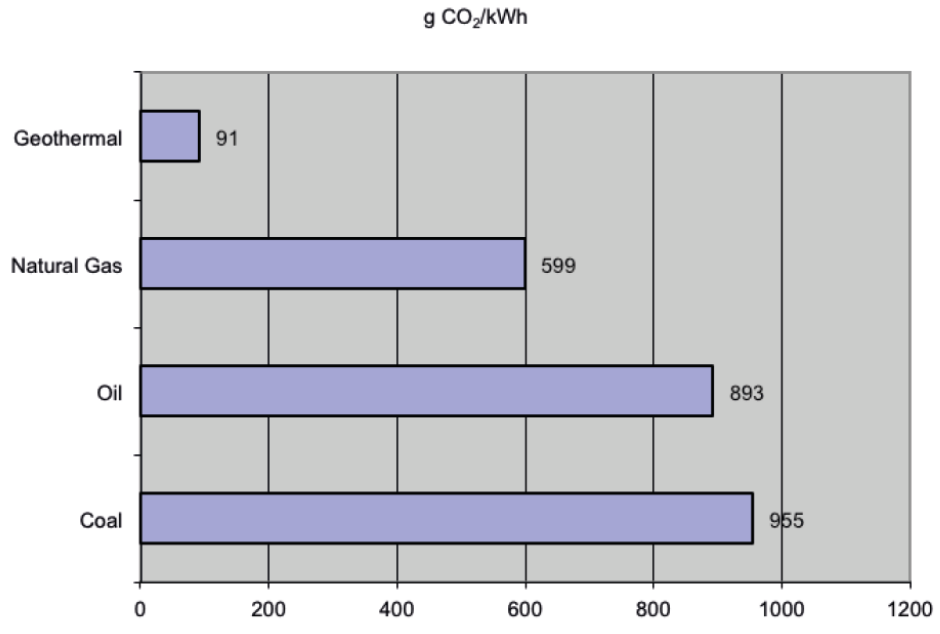


Figure 1: Comparison of CO<sub>2</sub> emissions from electricity generation by geothermal, natural gas, oil, and coal in the US in 2003.

The amount of carbon dioxide produced by geothermal energy production only accounts for 3.6% of the total carbon dioxide being produced; therefore it can be considered clean energy (Bloomfield et al., 2003). With an increase in the price for nonrenewable energy resources, and more countries striving to use clean energy, the use of renewable energy resources is anticipated to rise, accounting for 50% of our global energy supply by 2040 (Demirbas, 2009). Geothermal energy production is not limited by highly variable meteorological conditions such as wind and sunlight (Fossoul et al., 2011), though it is affected by geology, heat flow, and the presence of water or lack thereof (Glassley, 2010).

A key limitation preventing the increased use of geothermal resources is the difficulty in locating the essential geologic setting in which energy can be productively and economically harnessed. Low enthalpy geothermal resources suitable for development of geothermal energy are generally characterized by a shallow, permeable groundwater reservoir with temperatures ranging from 80-150°C (Chandrasekharam and Bundschuh, 2008). This type of setting is generally only found in volcanic regions and specific tectonic settings, such as subduction zones, spreading centers, and hot spots. The research presented in this document is focused on the Basin and Range province of the western United States, a rift basin formed behind a volcanic front that formed at a subduction zone. A subduction zone is commonly characterized by an oceanic plate being pushed by a spreading center beneath a less dense continental plate. It is theorized that the process of tectonic subduction creates small scale convection cells above the descending tectonic plate (Hart, Glassley, and Karig 1972). The upwelling of these convection cells causes spreading that creates rift basins like the Basin and Range province of the United States, which exhibits heat flow in localized areas near the surface exceeding 150 mW/m<sup>2</sup> relative to the average global heat flow at the surface of 87 mW/m<sup>2</sup> (Glassley, 2010).

Another limitation of geothermal energy is the cost of exploration. Production drilling can be an expensive step in the exploration process, and is usually only conducted after substantial evidence is presented to support the presence of a geothermal resource at depth. For example geochemistry, geophysics, and remote sensing can all be used as tools to evaluate the potential for the presence of a geothermal system before

production drilling is conducted. Since drilling is one of the most expensive steps in exploration, slim holes (diameters less than 15 cm) are commonly drilled to depths of around 2000 m to profile temperatures at depth (Glassley, 2010). Downhole equipment can be used to take rapid temperature measurements at various depths, and cores taken during drilling can be used to calculate thermal conductivity of the rock. The temperature profile is used to calculate the geothermal gradient. Despite these methods the exploration process is costly due to the cost of multiple slim holes that must be drilled in the exploration process, as well as the temperature gradient drilling and production drilling conducted in the later phase.

To decrease the amount of drilling into areas of unknown geothermal resource potential, rapid shallow (two meters) temperature measurements have been used in the Basin and Range to identify areas which may overlie deeper thermal reservoirs (Coolbaugh et al., 2007). The process of collecting shallow temperature measurements is done by driving a steel rod two meters into the ground, placing a thermocouple probe in the rod shaft, and measuring the temperature after it has equilibrated (Sladek et al., 2007). Shallow temperature measurements have been shown to be a reliable exploration tool in the Basin and Range province of the western United States through extensive use in the field (LeSchack and Lewis, 1983). However, there have been cases where these measurements have been proven unreliable, as discussed in the related work section of this document.

These two-meter temperature measurements can also be effectively used to gain insight into the horizontal temperature patterns between areas where temperature gradient

drilling is conducted (LeSchack and Lewis, 1983). A better understanding of the relationship between the shallow two-meter temperature and the deeper (>100 meters) temperature could aid in locating potential geothermal resources (Coolbaugh et al., 2007).

## **1.2 General Geothermal Concepts**

The Earth's core reaches temperatures of approximately 4,900°C, due to the heat created from the formation of Earth and the decay of radiogenic elements which produce heat (Glassley, 2010). This temperature is only an approximation due to the inability to directly measure the temperature of the Earth's core. Heat constantly flows from the Earth's interior to its crust producing enough energy to potentially create 42 million megawatts of power (Blodgett and Stack, 2009). It is this heat which is the major driving factor for the presence of geothermal systems. The pressure and temperature in geothermal systems in use and under consideration for electricity production generally control whether hydrothermal reservoirs are liquid water dominated, as in most cases, water vapor dominated, or sometimes both (Bodvarsson et al., 1986).

Heat is transported through geothermal systems primarily through convection in flowing groundwater and secondarily through conduction in static groundwater (Freeze and Cherry, 1979). Conduction not only transports heat through static groundwater, but also through the bedrock and less permeable units in a geothermal system. Conductive heat transport can be described as the transfer of heat from high temperature areas to lower temperature areas in the absence of fluid movement. Conduction of heat in a solid, liquid, or gas can be expressed by Fourier's law, which linearly relates heat flux to the temperature gradient:



$$H_{\beta} = -\lambda_{\beta} \nabla T_{\beta} \quad (1.1)$$

where  $H_{\beta}$  is heat flux,  $\nabla T_{\beta}$  is the three dimensional temperature gradient,  $\lambda$  is the thermal conductivity of the media, and  $\beta$  represents the fluid phase (i.e. liquid or gas). For this equation, it is assumed that the solids and the liquids are the same temperature (Domenico and Schwartz, 1990). A negative sign is placed in front of thermal conductivity to represent heat flowing toward the lower temperature (Naterer, 2002).

There are three types of convection: forced, free, and mixed convection. Fluid motion caused by differences in the pressure gradient, as described by Darcy's law, causes forced convection. Fluid and heat flow in geothermal systems can also be controlled by the properties of faults, rock layers, and the location of recharge and discharge zones (Bodvarsson et al., 1986). Darcy's law can be used to model free convection as well. Free convection is commonly the more dominant fluid motion in hydrothermal systems (Domenico and Schwartz, 1990). Free convection is caused by differences in fluid density due to the temperature gradient, with the hotter, less-dense fluid rising and the cooler fluid moving into its place creating a buoyancy effect (Domenico and Schwartz, 1990). Mixed convection is a combination of both forced and free convection.

Understanding the governing equations of fluid flow in a porous medium is an important factor in the understanding convective processes in a geothermal reservoir (Cheng, 1978). This research is focused on the multiphase flow of liquid water, water vapor, air, and heat through a two-dimensional porous medium. Darcy's law can be used

to describe the flow of fluid in a homogeneous porous media. Darcy's law for multiphase flow is

$$q_{\beta} = -k \frac{k_{r\beta}(S_{\beta})}{\mu_{\beta}} (\nabla P_{\beta} - \rho_{\beta} g), \quad (1.2)$$

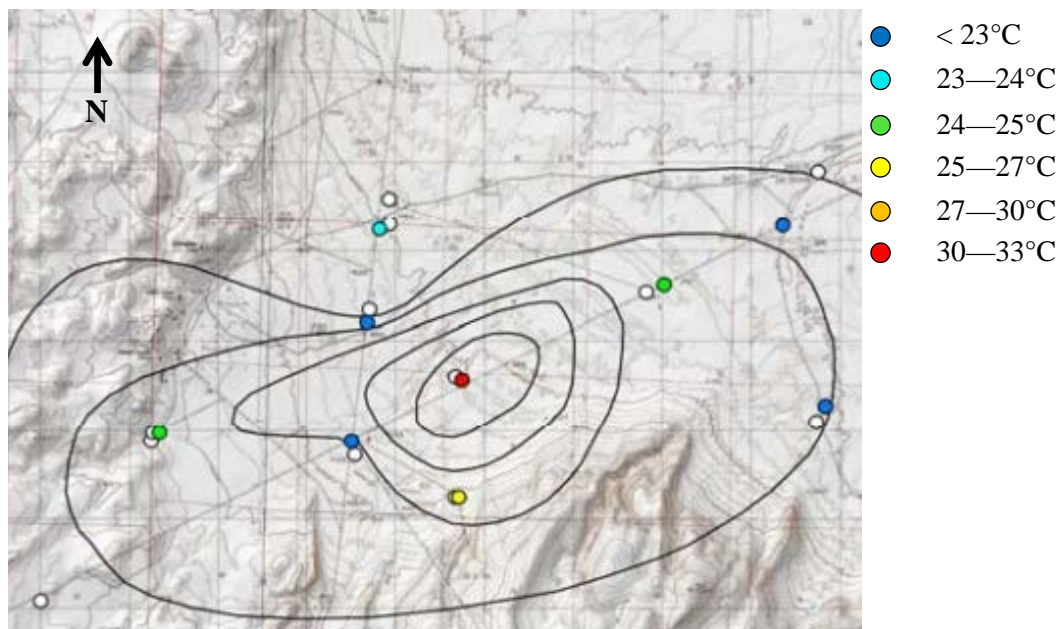
where  $\beta$  represents the fluid phase,  $q_{\beta}$  is Darcy velocity of phase  $\beta$ ,  $k$  is intrinsic permeability of the porous medium,  $k_{r\beta}$  is relative permeability of phase  $\beta$ ,  $\mu_{\beta}$  is dynamic viscosity,  $\rho_{\beta}$  is density of the fluid phase,  $S_{\beta}$  is saturation of phase  $\beta$ ,  $\nabla P_{\beta}$  is pressure gradient of phase  $\beta$ , and  $g$  is the gravitational acceleration. There is a negative sign in front of the potential energy term ( $\rho_{\beta} g$ ) to represent the downward direction which the vertical dimension increases in the coordinate system.

### 1.3 Related Work

A simple method of looking for temperature anomalies during geothermal exploration is the use of thermal remote sensing to map surface temperatures. These surface temperature measurements can be taken quickly over a large area, although they are greatly affected by solar radiation, vegetation, and climate (Coolbaugh et al., 2007). To avoid the effects of solar radiation and vegetation, one-to two-meter temperature measurements are commonly taken to locate geothermal anomalies. One to two-meter temperature measurements have been extensively used in the western United States to locate geothermal anomalies since 1973, but there have been few modeling studies testing how these shallow temperature measurements correlate to deeper temperatures (Olmsted and Ingebritsen, 1986).

Two-meter temperature measurements do not always effectively delineate temperature anomalies at greater depths, and this is likely due to the spatial variability of parameters that affect heat flow to the surface (Olmsted and Ingebritsen, 1986). The United States Geological Survey (USGS) conducted multiple one-meter temperature surveys from 1973 to 1985 at both Soda Lakes and Upsal Hogback geothermal areas in the western Carson Desert, Nevada. The one-meter temperature measurements collected were compared to temperatures measured in USGS wells at depths of 15-45 meters to determine if the horizontal temperature variability at the near surface is correlated to spatially varying temperature at depth. The one-meter temperature measurements taken at Soda Lakes effectively outlined the temperature patterns at depth, but the one-meter temperature measurements at Upsal Hogback did not. Not only did the Upsal Hogback area have significantly less heat flow at the near-surface, but there were several perturbing factors unrelated to increased temperature at depth that affect temperature at one meter depth (Olmsted and Ingebritsen, 1986). These perturbing factors such as the areal variation of thermal diffusivity can affect temperature at one meter depth by more than 4°C. One reason thermal diffusivity can vary is due to changes in the soil or rock type that have different thermal conductivities. This study by Olmsted and Ingebritsen reveals the effects of factors such as thermal diffusivity on temperature at the near surface. Changes in temperature due to areal variations in the perturbing factors such as thermal diffusivity may be avoidable by taking deeper temperature measurements (Olmsted, 1977).

Two-meter temperature measurements have been used to successfully identify geothermal anomalies at both Desert Queen and Desert Peak geothermal areas (Coolbaugh et al., 2007). Both areas are in northwestern Churchill County, Nevada, where a relatively deep (60 meters) aquifer is overlain by dry, unconsolidated alluvium and colluvium. In the Desert Queen area, nine original temperature gradient wells drilled to 30 meters were compared to two-meter temperature measurements taken from the same locations. The thermal anomaly produced in both cases matched very well (Figure 2). While these and other surveys have shown the effectiveness of two-meter temperature measurements as an exploration tool, there have been few related studies done incorporating numerical modeling of variations in geologic and hydrologic properties to see how they affect temperature at shallow depths.



○ The white dot represents the locations where temperature gradient drilling was conducted.

⤿ The black lines represent temperature contours at a depth of 30 meters with 18°C separation

Figure 2: Comparison of two-meter temperature measurements to temperature at 30 meters depth at Desert Queen area. White dots represent 12 gradient wells and the black lines represent temperature contours at a depth of 30 meters with 18°C separation. The colored dots represent the two-meter temperature measurements; dark blue = <23°C, light blue = 23—24°C, green = 24—25°C, yellow = 25—27°C, orange = 27—30°C, red = 30—33°C. Image is from Coolbaugh et al., 2007.

The contours in Figure 2 are representative of the temperature pattern at depth.

The research presented for the study at the Desert Queen area did not explicitly state the exact temperatures at 30 meters depth where temperature gradient drilling was conducted, instead stating an 18°C separation between each contour. The highest temperature at two meters depth was found in the center of the nine temperature survey locations and the temperatures at 30 meters depth show the same location of highest temperature. This correlation in the temperature pattern between the temperature at 2 and 30 meters depth

indicates that the two-meter temperature surveys are successful at identifying temperature anomalies at depth in the Desert Queen geothermal area.

Although the temperature pattern at two meters depth correlates to the temperature pattern at 30 meters depth, they are not completely identical. A small discrepancy can be seen on the western side of Figure 2, where the western most green and dark blue dots do not correspond with the contours that represent temperature at depth. This indicates that while some temperatures at shallow depths are representative of the same temperature pattern at depth, there are subsurface heterogeneities that can cause differences between the temperature patterns.

#### **1.4 Purpose/Objective**

The use of shallow temperature surveys in the field is well documented and shown to be similar in comparison with deeper temperatures, although the link between temperature at depth and two meters is largely understudied. There have been many field studies testing the viability of two-meter temperature measurements but no modeling experiments testing the correlation between temperature at two meters and deeper temperatures. The purpose of this thesis is to use numerical modeling to test how different forms of spatial variability in geologic and hydrologic properties might horizontally displace temperature at two meters depth, as well as testing how variations in geologic and hydrologic properties affect heat flow in the geothermal system.

During geothermal exploration one might expect a two meter temperature measurement to be representative of temperature at depth, such that an isolated high

temperature geothermal anomaly at depth would be correlated with a high temperature anomaly directly above it at two meters depth as shown in Figure 3.

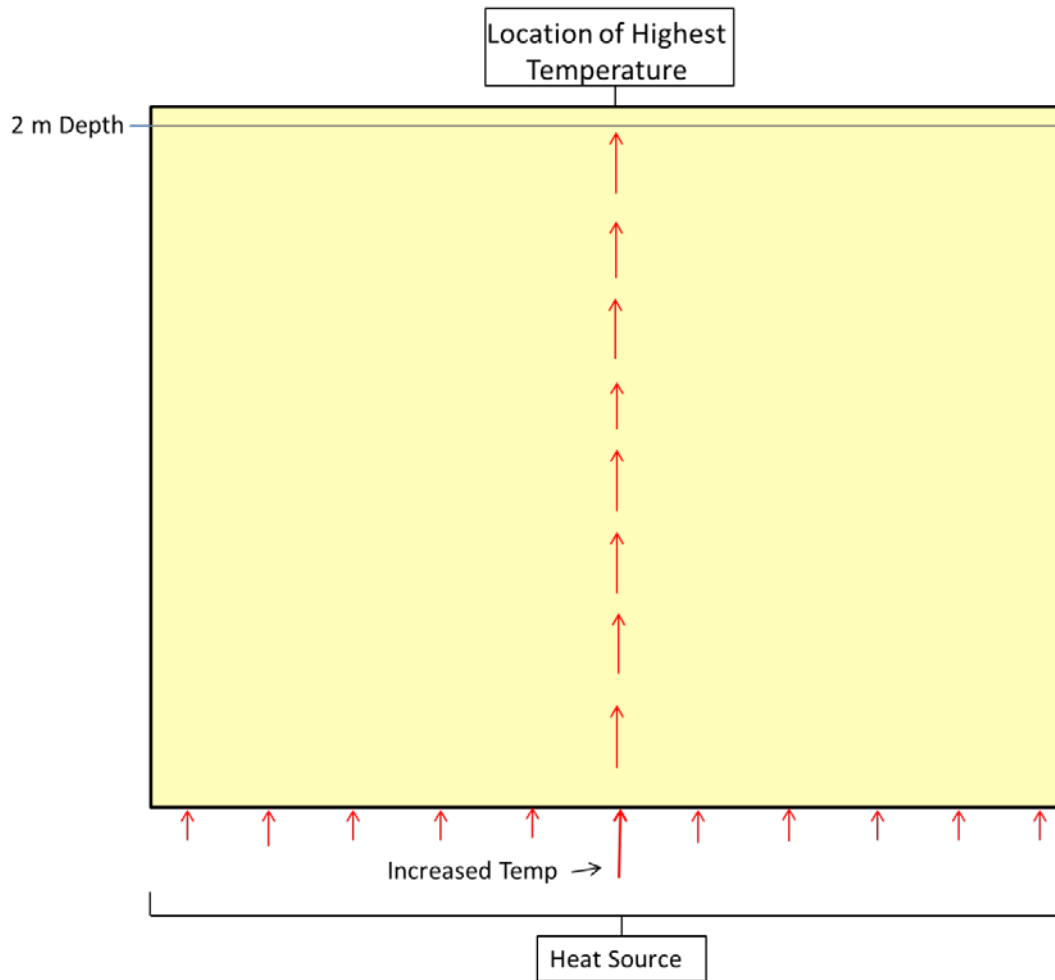


Figure 3: Conceptual image of an isolated geothermal anomaly in homogenous material.

It has been shown that this is not always the case and that there are many factors that can displace that temperature, such as structural and material heterogeneities (Coolbaugh et al., 2007). This study focuses on the effects of material heterogeneities and how they displace heat flow. Material heterogeneities are defined by bulk characteristics

of the rock such as permeability, thermal conductivity, or porosity. Testing how changes in these parameters can individually displace temperature provides a better understanding of what types of heterogeneities can result in misleading temperatures at shallow depths. The possible horizontal displacement by these simple heterogeneities is illustrated in Figure 4.

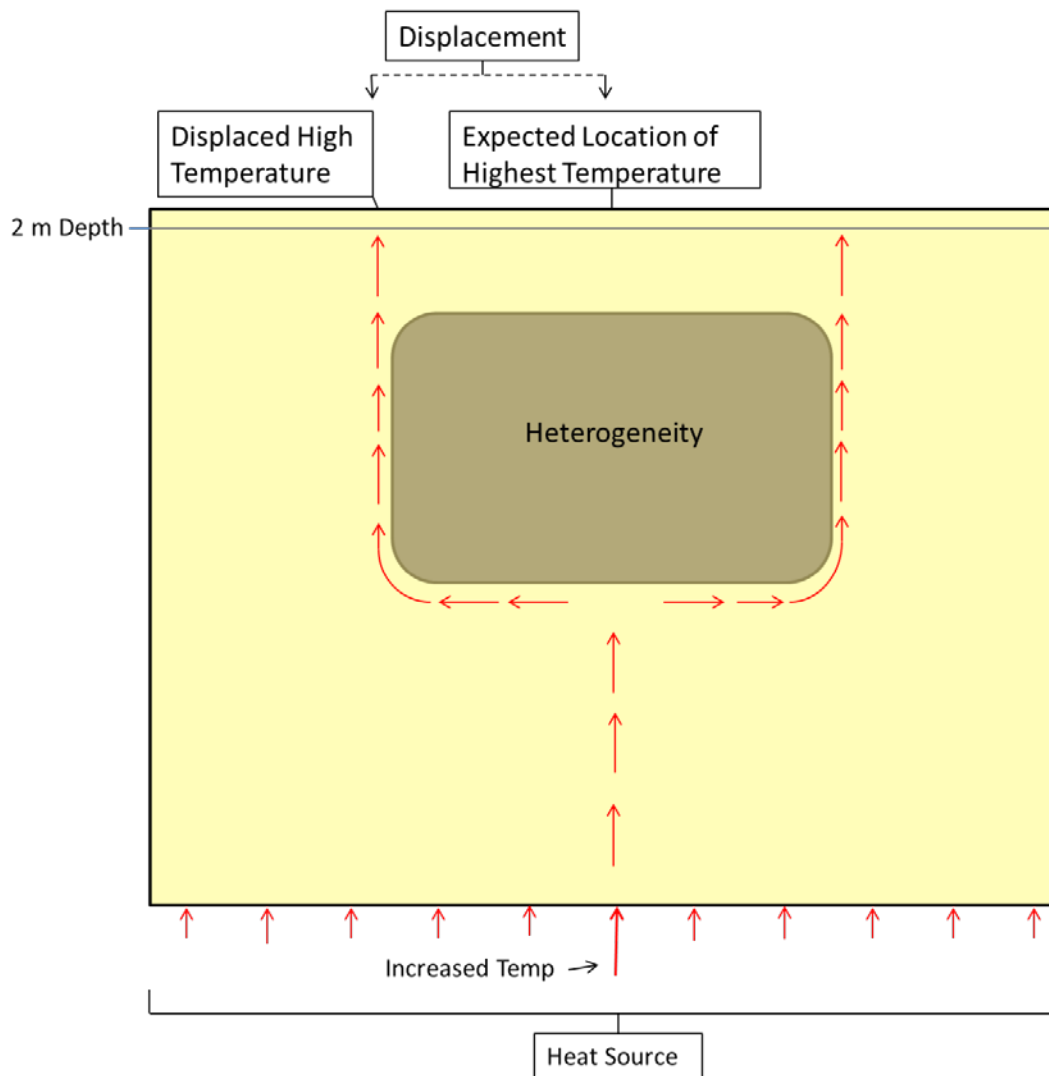


Figure 4: Conceptual image of an isolated geothermal anomaly in heterogeneous material.



The circumstance illustrated in Figure 4 may not only displace the temperature, but depending on the pattern of the heterogeneity, could also create preferential pathways that amplify the temperature. These material heterogeneities can not only displace temperature from an isolated and increased point source, but could also create the illusion of a geothermal anomaly at depth. Therefore, by testing a uniform and invariable heat source at the lower boundary with a heterogeneity in the subsurface, any displacement would be solely due to the variation of the parameters of that heterogeneity as shown in Figure 5.

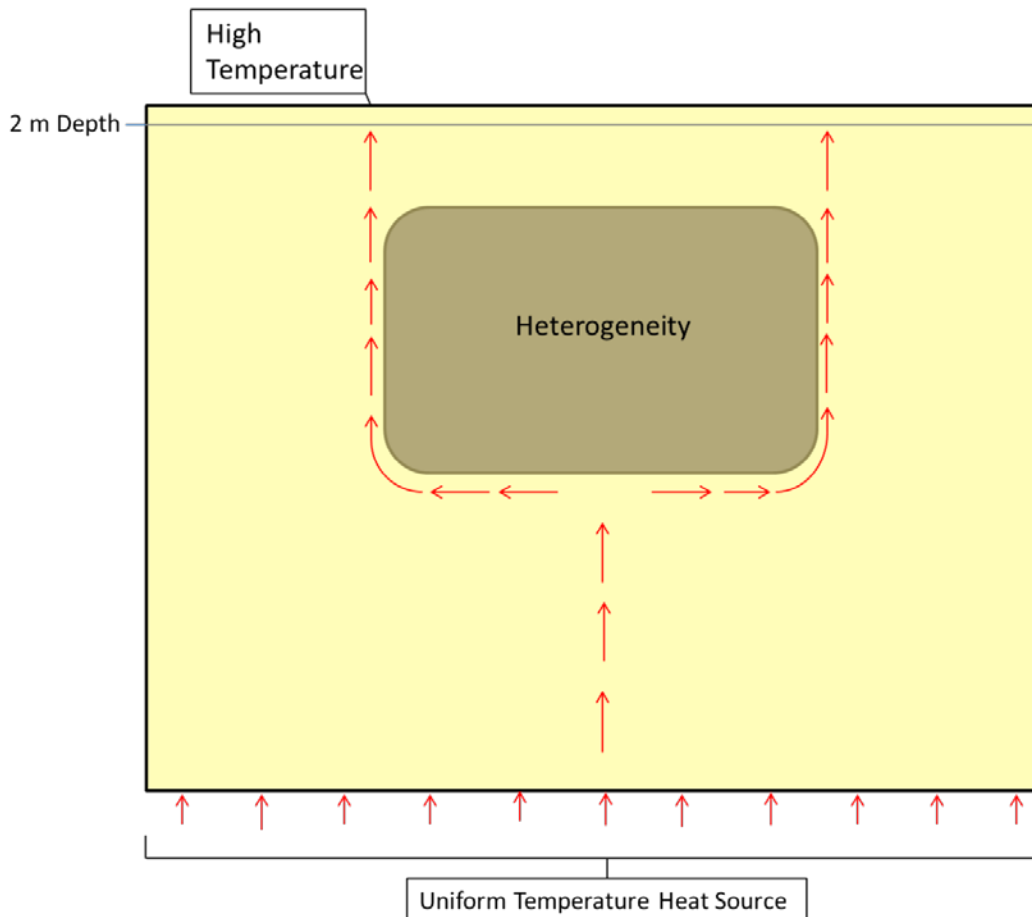


Figure 5: Conceptual image of a geothermal anomaly with uniform temperature at the lower boundary in heterogeneous material.

If results did not show a significant change in temperature at two meters depth in the horizontal direction with a uniform heat source at the lower boundary, that would provide additional support of two-meter temperature measurements as a useful exploration tool. Several parameters that have an effect on temperature were altered above an undeveloped geothermal reservoir to test how they affect temperatures at two meters depth. The parameters tested in this study are permeability, thermal conductivity of the rock, porosity and residual liquid saturation. The parameters tested were varied one at a time to see how each parameter individually affects the temperature. The testing of simple heterogeneous patterns of material properties can help to better understand the variability that might be expected in the field if one knows the range of that given parameter in that general area.

## CHAPTER 2

### METHODS

#### 2.1 TOUGH2

This study employed numerical modeling using TOUGH2 to test how altering the parameters controlling heat flow would affect temperature at two meters depth. Two of the major uses of TOUGH2 are geothermal reservoir engineering and flow and transport in variably saturated media and aquifers (Pruess, 1999), and both of these topics pertain to this research. In TOUGH2 the individual phase fluxes are given by the multiphase version of Darcy's law, written as

$$\mathbf{F}_\beta = \rho_\beta \mathbf{u}_\beta = -k \frac{k_{r\beta} \rho_\beta}{\mu_\beta} (\nabla P_\beta - \rho_\beta \mathbf{g}) \quad (2.4)$$

where  $\mathbf{u}_\beta$  represents the volume flux in each fluid phase,  $\mu_\beta$  is the viscosity of each fluid phase,  $k$  is the intrinsic permeability,  $\rho_\beta$  is the density of the fluid phase, and  $k_{r\beta}$  is the relative permeability of each fluid phase.  $P_\beta$  is the sum of the capillary pressure and the fluid phase pressure.

The heat flow was solved using the heat flux equation stated as

$$\mathbf{F}^{NK+1} = -\lambda \nabla T + \sum_\beta h_\beta \mathbf{F}_\beta \quad (2.5)$$

where  $\lambda$  represents thermal conductivity, and the  $h_\beta$  represents the specific enthalpy of each fluid phase. This first term on the right side of the equation ( $-\lambda \nabla T$ ) represents the conductive component and the second term ( $\sum_\beta h_\beta \mathbf{F}_\beta$ ) is the convective component of the

heat flux equation. It is these governing equations conveyed by Pruess et al. (1999) that control the flow of fluids and heat in the models conducted in this research.

TOUGH2 uses different equation of state (EOS) modules, each determining which fluids are in consideration and their fluid properties. The equation of state module used for this research is EOS3, which can model the flow of water and air. The EOS3 module is ideal for the modeling in this research as the fluids of interest are water, water vapor and air. This EOS also allows for the analysis of heat flow through a geothermal system.

## **2.2 Model Domain and Boundary Conditions**

The process of heat transport from a deeper (>100 feet deep) reservoir to the near surface was simulated in a partially saturated vertical column. The model mesh of this vertical column is 27 vertical grid cells by 25 horizontal grid cells. The upper and lower horizontal layer of grid cells are  $1.0 \times 10^{-6}$  meters in height and are used to impose the upper and lower boundary conditions. The smaller size of the boundary layers makes a negligible contribution to the total vertical depth of the model. The remaining grid cells are 4 x 4 meters in size for a 100 x 100 meter grid total (Figure 6). It is in these inner 625 grid cells that the geologic and hydrologic properties (permeability, thermal conductivity, porosity, residual liquid saturation) were altered in heterogeneous patterns to assess their effect on temperature at two meters depth and heat flow from the deeper heat source to two meters depth.

The upper boundary layer represents the Earth's surface and was given a constant temperature of 20°C, a general average air temperature for the Basin and Range region of the United States. The lower boundary row represents the geothermal reservoir and was given a constant temperature of 95 °C, which is considered to be on the lower end of temperatures found in a geothermal system, and which is realistic for depths of 100 meters in the Basin and Range of the United States (Glassley, 2010). These conditions are similar to those found at the Desert Queen geothermal area and the Astor Pass geothermal system (Coolbaugh et al., 2007; Reeves et al., 2012). Temperatures at the upper and lower boundary were held constant by assigning them an overwhelmingly large heat capacity, such that finite rates of heat exchange would cause negligible temperature change.

The pressure at the upper boundary was set to 100 kPa, representative of atmospheric pressure. The volume of the upper boundary layer was increased to prevent the pressure from changing, as changes in atmospheric pressure are negligible relative to those below the surface. The increased volume and decreased size of the upper boundary cells ensures that they will not be included in the global material balances (Pruess, 1999). The volume at the lower boundary layer was defined by the dimensions of the grid cells, and pressures were therefore allowed to change. Permeability at the larger upper boundary was decreased to prevent the exchange of fluids between the boundary layer and the inner model. If the fluid in the upper boundary were allowed to interact with the inner model domain, it would easily fully saturate the model due to its increased volume. Figure 6 shows the two dimensional model domain described above.

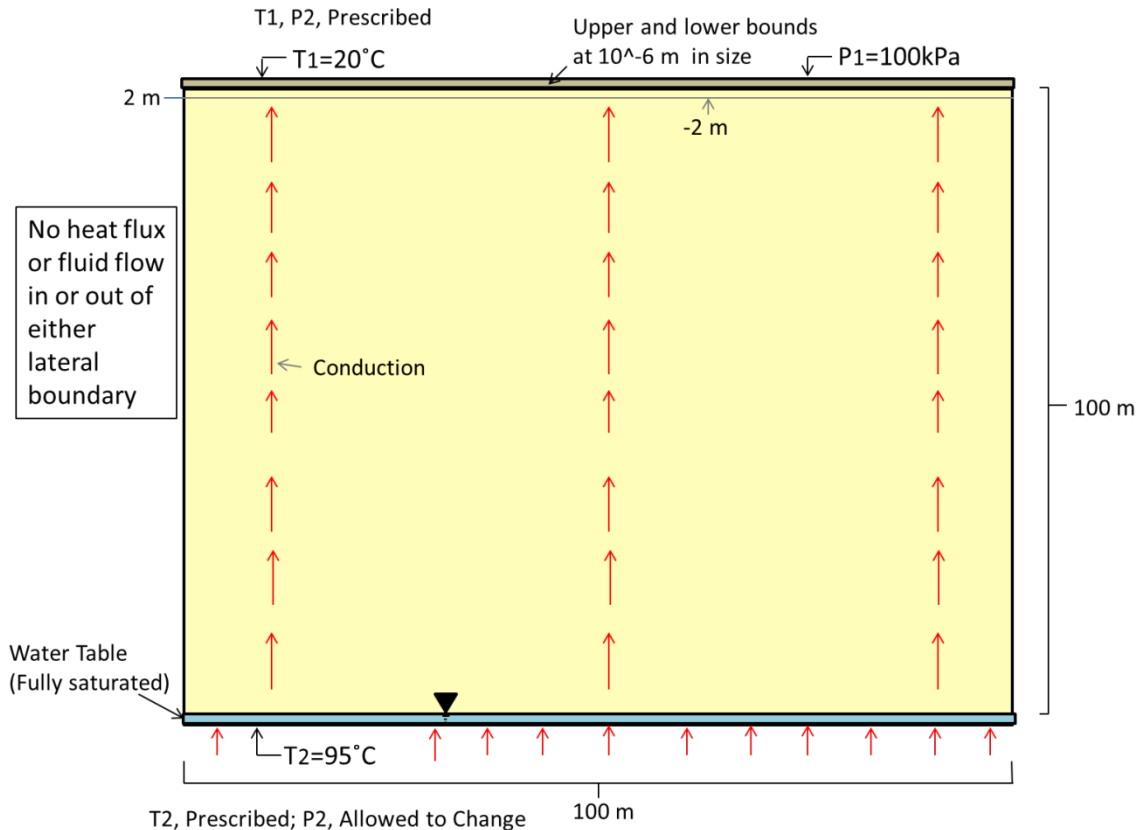


Figure 6: Homogeneous 2D model diagram showing model dimensions, initial boundary temperatures and conductive heat flow.

The inner yellow section of the model diagram above represents the 25x25 cell area in which the various parameters tested such as intrinsic permeability; thermal conductivity, porosity, and residual liquid saturation were altered individually to assess their impact on the temperature at two meters depth at steady state. Three types of spatial patterns were used to test a high and low value from a realistic range for each of the parameters tested. The three spatial patterns tested were homogeneous, large checkerboard pattern, and vertical layers pattern. The large checkerboard pattern consists of alternating sections of 5 x 5 grouped cells (20 x 20 meters) in which the parameters

were tested. The vertical layers pattern consists of alternating columns of 1 x 25 cells in which the parameters were tested. Initial testing of small checkerboard and horizontal layers spatial variations indicated that the heterogeneities were not significant enough to cause a horizontal disturbance in temperatures. In the homogeneous model the parameters being tested were changed one at a time in the entire model domain while all other parameter values remain as the default.

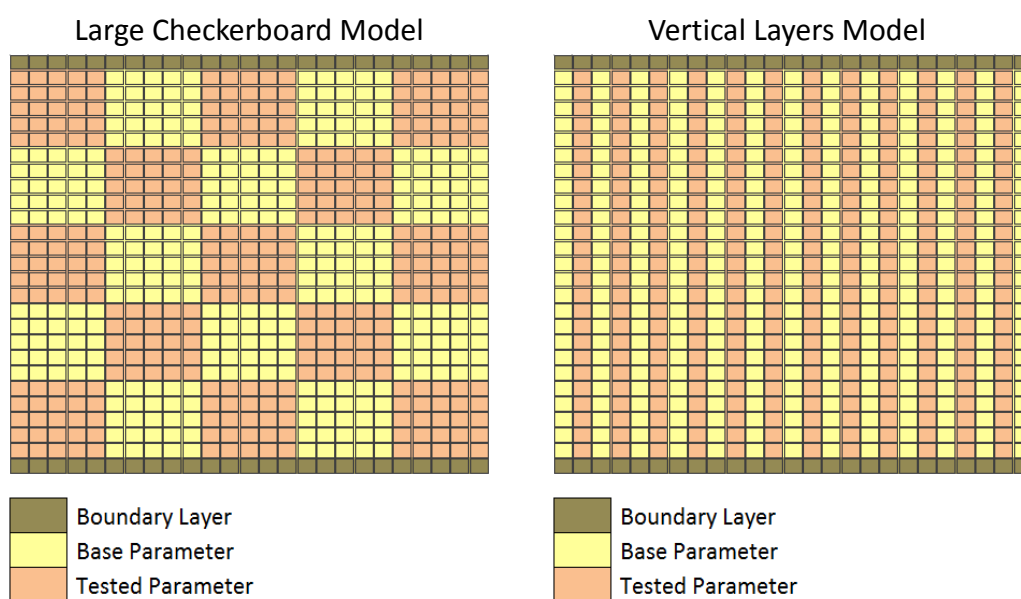


Figure 7: Heterogeneous patterns in which the parameters tested are altered.

In the large checkerboard and the vertical layers models (Figure 7) the parameters tested were altered in heterogeneous patterns to better understand how they might affect heat flow to two meters depth. Both models alter the parameters in heterogeneous patterns and were chosen for their ability to horizontally displace the vertical transport of heat. The subsurface is generally always heterogeneous and groundwater modelers often

make assumptions and simplifications to be able to predict groundwater flow (Kresic, 2006).

### **2.3 Modeling Methods and Initial Conditions**

For this research there was no specific study site of interest so the choice for rock/sediment type to be modeled in the subsurface was arbitrary. Sand was chosen as the media through which water, air, and heat would be transported. The base parameters were set to represent medium grain sand, commonly found as basin fill alluvium in the Basin and Range of the United States. Of the base parameters, permeability, thermal conductivity, porosity, and residual liquid saturation were altered systematically one at a time.

The geologic parameters were set to represent medium-course grain sand. The rock grain density was set to  $2000 \text{ kg/m}^3$  to simulate this sand. Porosity for sands generally ranges from 0.25 to 0.50 (Freeze and Cherry, 1979). Baseline porosity was set to 0.45 which is at the higher range of porosity given by Freeze and Cherry (1979) and is representative of a medium to coarse grain sand. Permeability was set to  $10^{-11} \text{ m}^2$  which is the median permeability value for sand given by Freeze and Cherry (1979) and was tested along a range from  $10^{-12} \text{ m}^2$  to  $10^{-10} \text{ m}^2$ . Sand has thermal conductivities ranging from  $0.3 \text{ Wm}^{-1}\text{K}^{-1}$  to  $4.3 \text{ Wm}^{-1}\text{K}^{-1}$ , for this research a base thermal conductivity of  $2.0 \text{ Wm}^{-1}\text{K}^{-1}$  was used and was tested along a range of  $0.5 \text{ Wm}^{-1}\text{K}^{-1}$  to  $3.5 \text{ Wm}^{-1}\text{K}^{-1}$  (Raznjevic, 1976). The base residual liquid saturation was set to 0.045, which is



representative of sand (Simunek et al., 2005). The residual liquid saturation was tested along a range of 0.045 to 0.15.

<b>Modeling Simulations</b>				
	<b>Permeability (m<sup>2</sup>)</b>	<b>Thermal Conductivity (Wm<sup>-1</sup>K<sup>-1</sup>)</b>	<b>Porosity</b>	<b>Residual Liquid Saturation</b>
<b>Sim 1 - Base Model (Homogeneous)</b>	10 <sup>-11</sup>	2.0	0.45	0.045
<b>Homogeneous Model</b>				
<b>Sim 2 - Low Permeability</b>	10 <sup>-12</sup>	2.0	0.45	0.045
<b>Sim 3 - High Permeability</b>	10 <sup>-10</sup>	2.0	0.45	0.045
<b>Sim 4 - Low Thermal Conductivity</b>	10 <sup>-11</sup>	0.5	0.45	0.045
<b>Sim 5 - High Thermal Conductivity</b>	10 <sup>-11</sup>	3.5	0.45	0.045
<b>Sim 6 - Low Porosity</b>	10 <sup>-11</sup>	2.0	0.25	0.045
<b>Sim 7 - High Porosity</b>	10 <sup>-11</sup>	2.0	0.50	0.045
<b>Sim 8 - Moderate Liquid Saturation</b>	10 <sup>-11</sup>	2.0	0.45	0.10
<b>Sim 9 - High Liquid Saturation</b>	10 <sup>-11</sup>	2.0	0.45	0.15
<b>Large Checkerboard Model</b>				
<b>Sim 10 - Low Permeability</b>	10 <sup>-12</sup>	2.0	0.45	0.045
<b>Sim 11 - High Permeability</b>	10 <sup>-10</sup>	2.0	0.45	0.045
<b>Sim 12 - Low Thermal Conductivity</b>	10 <sup>-11</sup>	0.5	0.45	0.045
<b>Sim 13 - High Thermal Conductivity</b>	10 <sup>-11</sup>	3.5	0.45	0.045
<b>Sim 14 - Low Porosity</b>	10 <sup>-11</sup>	2.0	0.25	0.045
<b>Sim 15 - High Porosity</b>	10 <sup>-11</sup>	2.0	0.50	0.045
<b>Sim 16 - Moderate Liquid Saturation</b>	10 <sup>-11</sup>	2.0	0.45	0.10
<b>Sim 17 - High Liquid Saturation</b>	10 <sup>-11</sup>	2.0	0.45	0.15
<b>Vertical Layers Model</b>				
<b>Sim 18 - Low Permeability</b>	10 <sup>-12</sup>	2.0	0.45	0.045
<b>Sim 19 - High Permeability</b>	10 <sup>-10</sup>	2.0	0.45	0.045
<b>Sim 20 - Low Thermal Conductivity</b>	10 <sup>-11</sup>	0.5	0.45	0.045
<b>Sim 21 - High Thermal Conductivity</b>	10 <sup>-11</sup>	3.5	0.45	0.045
<b>Sim 22 - Low Porosity</b>	10 <sup>-11</sup>	2.0	0.25	0.045
<b>Sim 23 - High Porosity</b>	10 <sup>-11</sup>	2.0	0.50	0.045
<b>Sim 24 - Moderate Liquid Saturation</b>	10 <sup>-11</sup>	2.0	0.45	0.10
<b>Sim 25 - High Liquid Saturation</b>	10 <sup>-11</sup>	2.0	0.45	0.15
<b>Increased Isolated Temperature in the Large Checkerboard Model</b>				
<b>Sim 26 - Low Thermal Conductivity</b>	10 <sup>-11</sup>	0.5	0.45	0.045
<b>Sim 27 - High Thermal Conductivity</b>	10 <sup>-11</sup>	3.5	0.45	0.045
<b>Large Checkerboard Model with Reduced Vertical Domain</b>				
<b>Sim 28 - Low Thermal Conductivity</b>	10 <sup>-11</sup>	0.5	0.45	0.045
<b>Sim 29 - High Thermal Conductivity</b>	10 <sup>-11</sup>	3.5	0.45	0.045

Table 1: Modeling scenarios and how the parameters alter from the base model.

The yellow spaces in Table 1 represent the parameter that was changed from its base value in that given simulation while the other parameters were held constant. For

each of the initial 25 simulations (Table 1), with the exception of the base model, the parameters were varied spatially in a homogeneous model, vertical layers model, and large checkerboard model, for a total of 25 simulations. Four additional simulations tested a high and low thermal conductivity in the large checkerboard model: two (Simulations 26 and 27) with an increased isolated temperature source in the thirteenth column of 105 °C and the other two (Simulations 28 and 29) with a smaller 50 meter vertical domain. The sizes of the patterns in the smaller vertical domain model were kept the same, although the number of grid cells was doubled in the horizontal and vertical dimensions (2 x 2 meters rather than 4 x 4 meters).

The additional models were chosen for further testing based on the results of the initial 25 simulations. The purpose of the increased isolated temperature in the large checkerboard heterogeneity models was to test if the horizontal disturbances in temperature that are created by the heterogeneity would be further amplified by an isolated increased temperature. The purpose of the model with a smaller vertical domain was to test the effect on disturbances in temperature at shallow depths in the presence of a shallower geothermal reservoir.

All models were run in two steps. For the first model run the temperature at the lower and upper boundary were held constant at 20 °C and the model was run to steady state. The lower boundary was fully saturated to initially act as the water table/top of the geothermal reservoir. The upper boundary was assigned a liquid saturation of 0.1 to simulate the general moisture one might find at the surface/root zone. This initial model run allows for the inner vertical column's initial liquid saturation of 0.3 to settle due to

gravity creating a new, slightly higher water table. This model run also allows the pressure gradient to equilibrate since the pressure at the lower boundary is allowed to change.

The second model run was a subsequent continuation using the saved output conditions from the first run as the initial conditions in the second run. For the second model run the temperature on the lower boundary was increased to 95 °C and run to steady state to create the temperature gradient between the surface and the geothermal reservoir at 100 meters depth.

Each model was run to an effective steady state. Effective steady state for this study can be defined by the understanding that any further changes in the output were negligible and driven solely by the cyclical fluctuations of the convection cells that develop near the lower boundary, as shown by the analysis of the output at multiple time steps. The models were all set to run for 1 million years to ensure that steady state was achieved. Though not all models reached one million years, all models did reach an effective steady state. Models were quantitatively analyzed by comparing temperature values between the time steps to ensure that an effective steady state was achieved. The final output for each model was then analyzed to assess the impact of the tested parameter's effect on temperature at two meters depth. Observations were also made of the variation of heat flow patterns for the different models at depth.

## CHAPTER 3

### RESULTS

#### 3.1 Permeability Results

Changes in permeability of  $10^{-12} \text{ m}^2$  and  $10^{-10} \text{ m}^2$  (low and high permeability respectively) were tested in three model domains (homogeneous, large checkerboard, and vertical layers) for a total of six simulations outlined in Table 1 as simulations number 2, 3, 10, 11, 18, and 19. Of the six model simulations testing permeability none showed significant horizontal change in temperature at two meters depth. The greatest horizontal change in temperature at two meters depth of  $0.01^\circ\text{C}$  occurred in the homogeneous model with a permeability of  $10^{-10} \text{ m}^2$  and can be considered negligible. However, temperatures at two meters depth did increase approximately  $0.5^\circ\text{C}$  from the low permeability scenarios to the high permeability scenarios. The results for all models testing changes in permeability are shown in Figures 8-10. Note that vector scales in each plot are representative of the maximum magnitude exhibited within that plot and all vectors originate from the center node of each grid cell, sometimes causing the vector head to exit the plot domain.

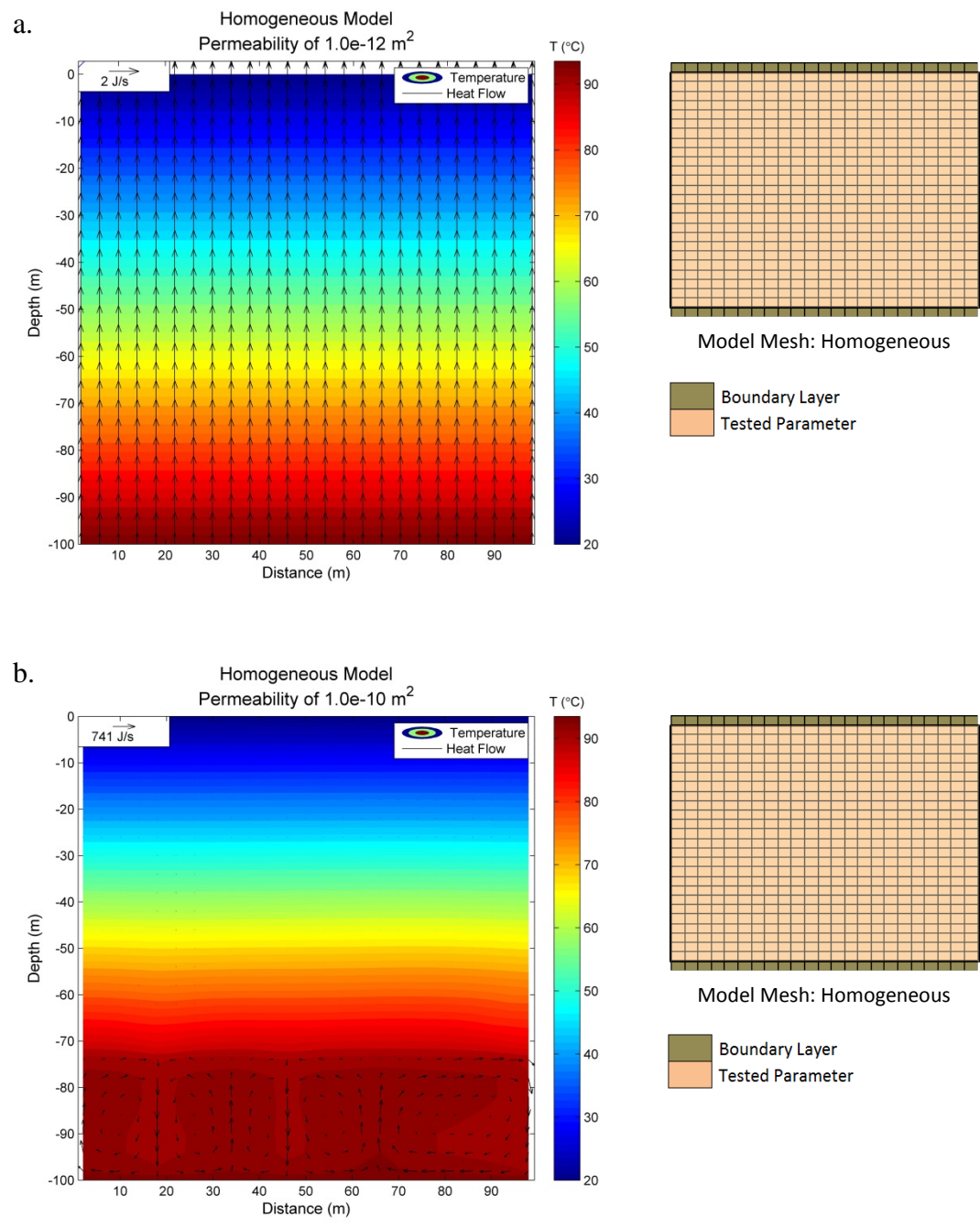


Figure 8: Results of the permeability simulations in a homogeneous model domain. Colored temperature contours are shown in °C and are overlain by heat flow vectors. a) Simulation 2 - Low permeability ( $10^{-12} \text{ m}^2$ ) with heat flow up to 2 J/s; b) Simulation 3 - High permeability ( $10^{-10} \text{ m}^2$ ) with heat flow up to 741 J/s.

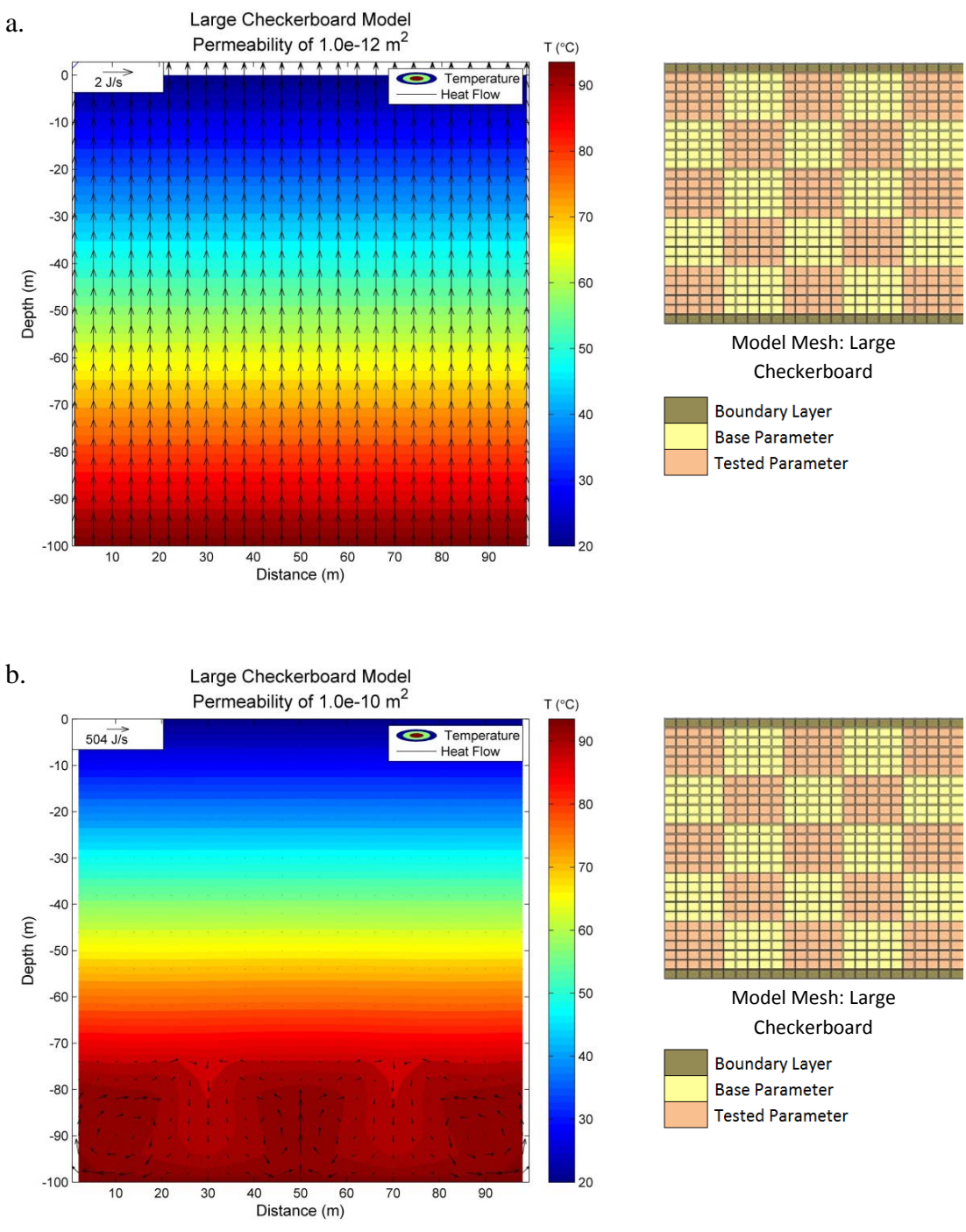


Figure 9: Results of the permeability simulations in a large checkerboard model domain. Colored temperature contours are shown in °C and are overlain by heat flow vectors. a) Simulation 10 - Low permeability ( $10^{-12} \text{ m}^2$ ) with heat flow up to 2 J/s; b) Simulation 11 - High permeability ( $10^{-10} \text{ m}^2$ ) with heat flow up to 504 J/s.

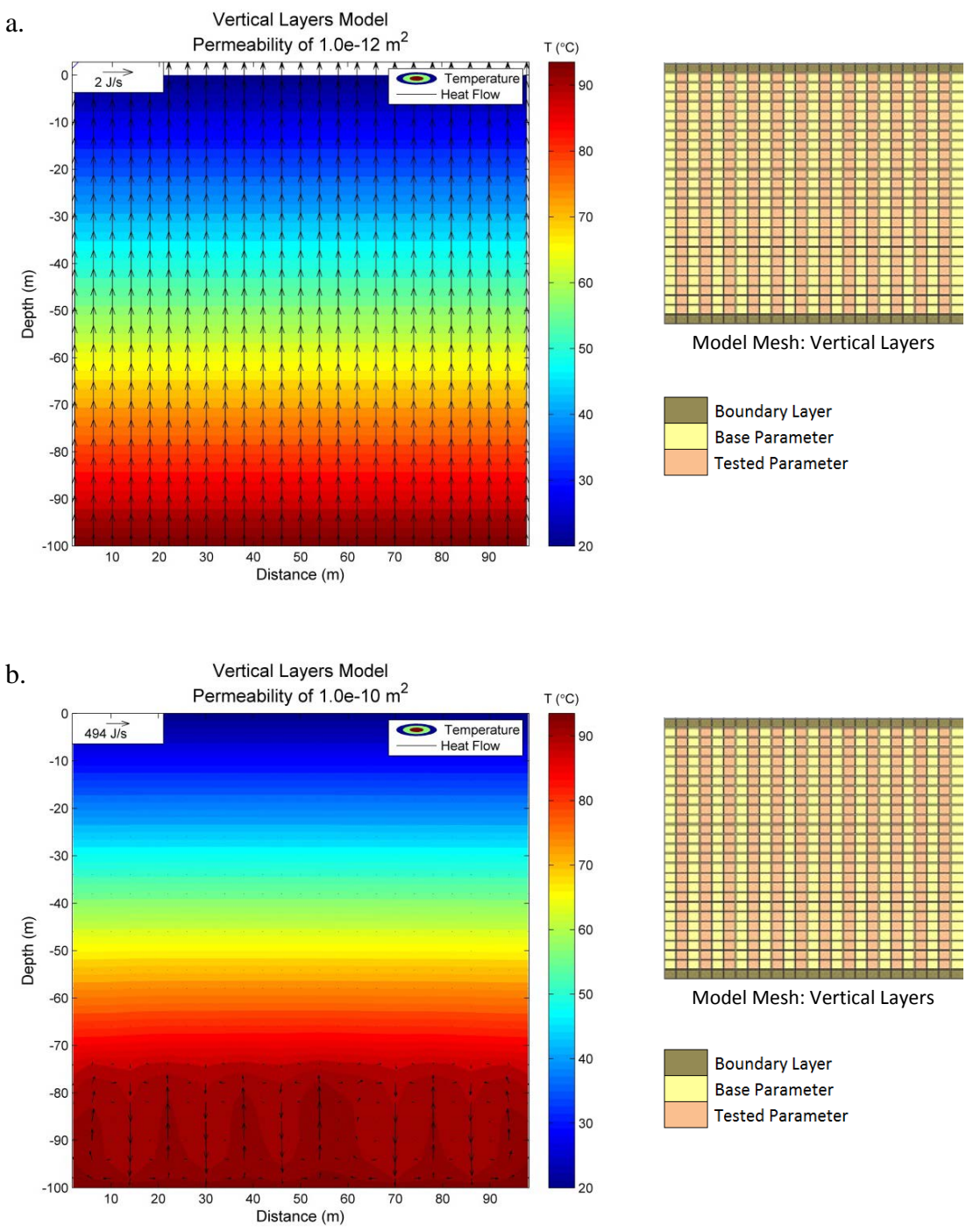


Figure 10: Results of the permeability simulations in a vertical layers model domain. Colored temperature contours are shown in °C and are overlain by heat flow vectors. a) Simulation 18 - Low permeability ( $10^{-12} \text{ m}^2$ ) with heat flow up to 2 J/s; b) Simulation 19 - High permeability ( $10^{-10} \text{ m}^2$ ) with heat flow up to 494 J/s.

The increase in temperature at two meters depth between low permeability models and high permeability models is due to the different methods of heat transport. For all low permeability simulations, heat flow is dominated by conduction (Figures 8a, 9a, and 10a). These low permeability simulations show a uniform horizontal temperature of 21.5 °C at two meters depth, with heat flux reaching only 2 J/s. The maximum heat flow is only 2 J/s because convection does not occur, due to the rocks inability to transmit fluid at a high enough velocity. Convective heat flow can be seen in all high permeability simulations (Figures 8b, 9b and 10b) in areas saturated with liquid and can reach heat fluxes of 741 J/s. While there is convection in the lower, liquid dominated portion of the domain, heat transport above the convection cells is primarily conduction. With respect to the heat flow vectors displaying 741 J/s, the smaller 2 J/s heat flow vectors above the convecting fluid are so small in comparison that they do not show up on the plots, as seen in Figures 8b, 9b and 10b. The homogenous, high permeability model (Figure 8b) shows a non-symmetrical pattern of circulating heat flow, due to the lack of spatial variation in the parameter being tested. Without changes in permeability from cell to cell the homogeneous, high permeability model does not develop a preferential flow pattern and becomes non-symmetrical with a larger convection cell on the right than on the left. In the large checkerboard and vertical layers models with altered high permeability (Figures 9b and 10b), the heat flow follows preferential pathways through the areas of higher permeability creating relatively symmetrical patterns compared to the homogeneous model (Figure 8b).



While all three high permeability models (Figures 8b, 9b and 10b) showed convection occurring in the lower portion of the model domains, the large checkerboard model showed the most significant difference in temperature horizontally of  $4.2^{\circ}\text{C}$  in the lower model domain at 82 feet below the surface. The convective heat flow for this model can be seen circulating through areas that are saturated with liquid in Figure 11.

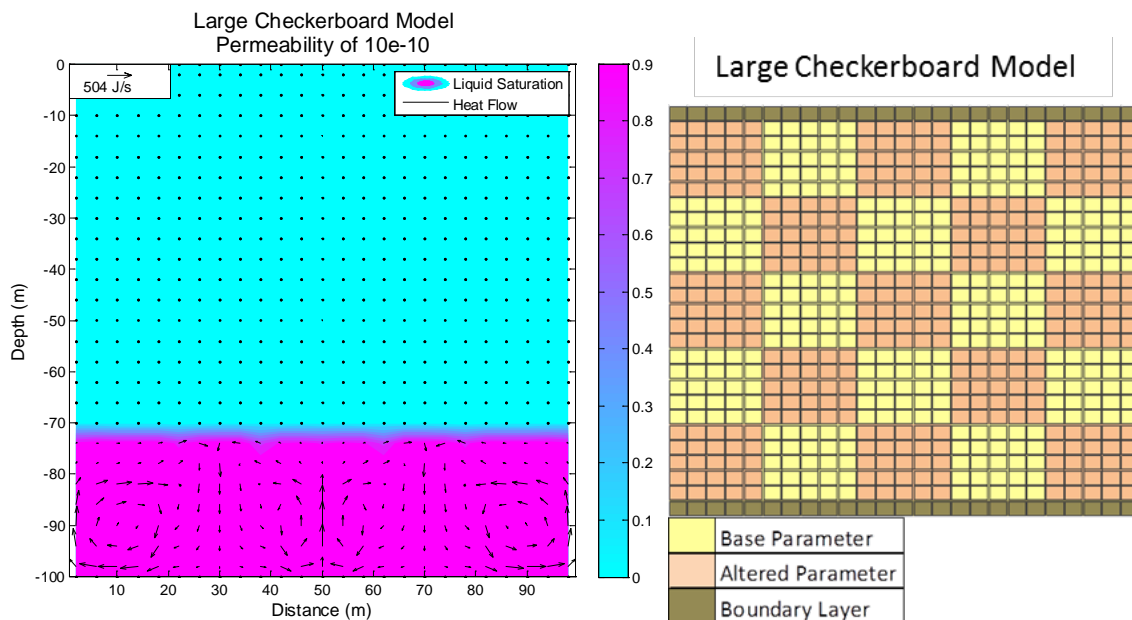


Figure 11: Heat flow vectors overlaying a liquid saturation plot for a large checkerboard model with high permeability (Simulation 11) next to the large checkerboard model pattern. This is the same model as 9b, showing liquid saturation instead of temperature.

The convection showed in Figure 11 occurs primarily in the area that is saturated with liquid, and is liquid dominated (i.e., heat flow and liquid convection share the same pattern). Heat moves vertically upward in the sections of the large checkerboard pattern with a higher permeability of  $10^{-10} \text{ m}^2$  and flows back down through the sections of the

large checkerboard pattern with a lower/base permeability of  $10^{-11} \text{ m}^2$ , as shown in Figure 11.

The existence of convective heat flow can be supported by analyzing the liquid velocity vectors for these simulations, as the liquid velocity vectors in the high permeability checkerboard simulation (Figure 12) show the same pattern as the heat flow vectors for this simulation (Figure 9b). Additionally, results show a significantly higher liquid velocity in the high permeability simulations in comparison to the low permeability simulations. The liquid velocity of large checkerboard model with altered high permeability is compared to the liquid velocity of the large checkerboard model with altered low permeability in Figure 12.

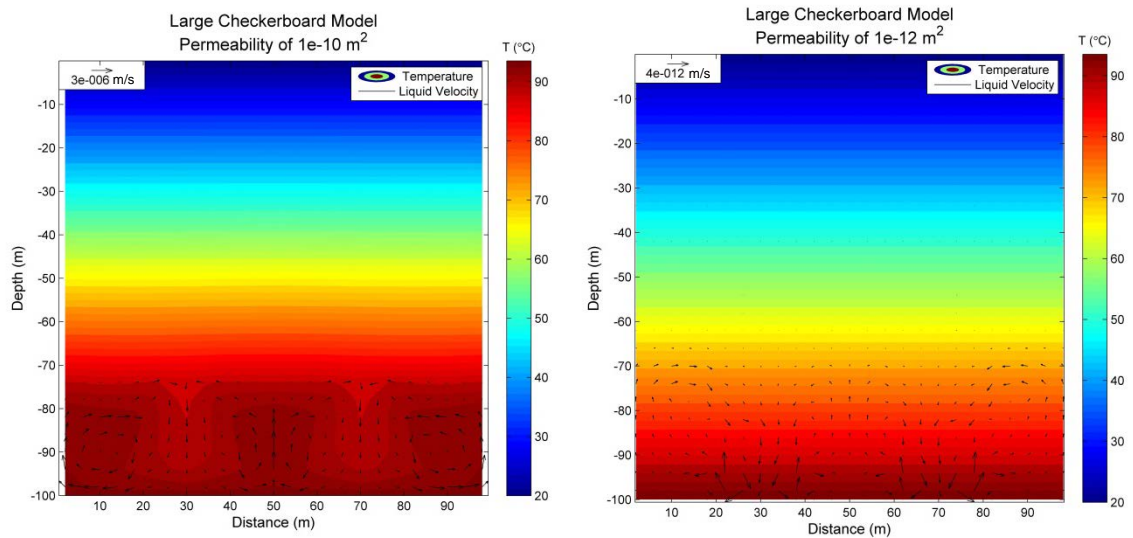


Figure 12: Temperature plot of the large checkerboard model with high permeability ( $10^{-10} \text{ m}^2$ ) (Simulation 11) on the left and low permeability ( $10^{-12} \text{ m}^2$ ) (Simulation 10) on the right overlain by liquid velocity vectors. Temperature is in  $^{\circ}\text{C}$ .

The liquid velocity in the large checkerboard model testing high permeability is six orders of magnitude greater than in the model with low permeability. The liquid circulation in the high permeability model moves at almost a foot per day, while the flow of liquid in the low permeability model is negligible in comparison. Liquid velocity exhibited similar conditions in all other models with circulating heat flow. The gas velocity for the same models presented in Figure 12 circulates above the water table at similar speeds, shown in Figure 13. Note that while gas appears to convect in the low permeability simulation shown in Figure 13 (image on the right) it is actually moving at a velocity of one micron per year, making it essentially motionless.

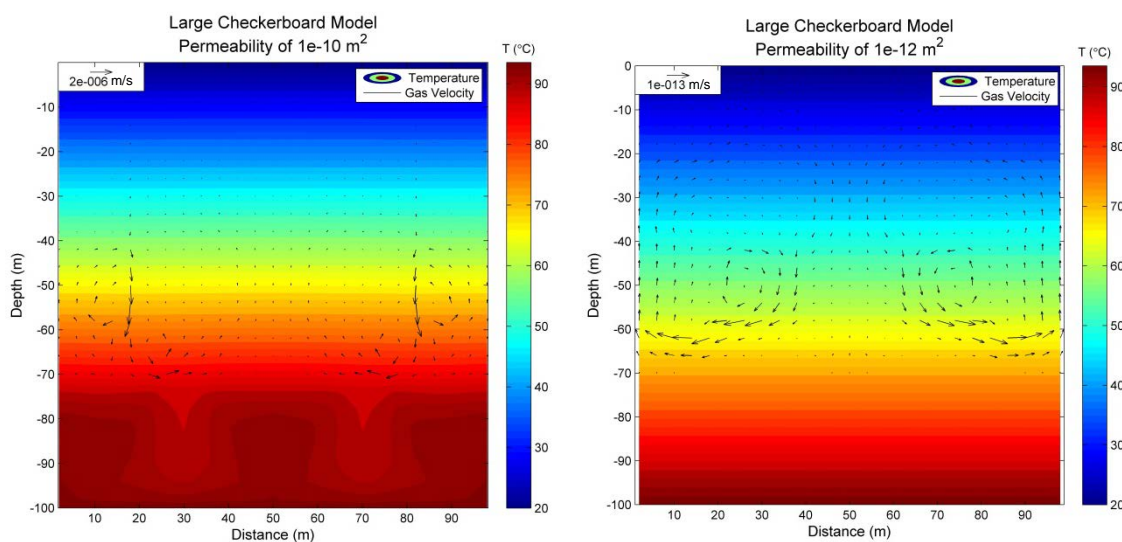


Figure 13: Temperature plot of the large checkerboard model with altered high permeability ( $10^{-10} \text{ m}^2$ ) (Simulation 11) on the left and altered low permeability ( $10^{-12} \text{ m}^2$ ) (Simulation 10) on the right overlain by gas velocity vectors. Temperature is in  $^{\circ}\text{C}$ .

While the gas velocities shown in Figure 13 exhibit speeds similar to that of the liquid velocities in Figure 12, gas migration does not affect heat flow and is not a

significant mechanism for heat transport in this research. The areas with the highest gas velocities do not exhibit disturbances in the temperature, therefore supporting the idea that gas velocity has no effect on heat flow. The circulating heat flow in Figure 9b shows a similar pattern to the liquid velocity in Figure 12, but not the gas velocity in Figure 13.

An additional way to test whether this circulation of fluid is truly convection is to calculate the Rayleigh number. A Rayleigh number indicates the propensity for free convection to occur (Wood and Hewett, 1982). The Rayleigh number is calculated using the following equation

$$Ra = \frac{kg\alpha(\rho C)_f L \Delta T}{\nu \lambda^*} \quad (3.1)$$

where  $k$  is permeability,  $g$  is gravitational acceleration,  $\alpha$  is the volumetric thermal expansion coefficient of the fluid,  $(\rho C)_f$  is volumetric heat capacity of the fluid,  $L$  is thickness of the porous layer,  $\Delta T$  is temperature difference across the layer,  $\nu$  is kinematic viscosity of the fluid, and  $\lambda^*$  is effective thermal conductivity of the fluid-filled medium. Effective thermal conductivity is defined by

$$\lambda^* = \lambda_{\text{fluid}}^{\phi} \lambda_{\text{solid}}^{(1-\phi)} \quad (3.2)$$

where  $\phi$  is porosity in an empirical model by Combarous and Bories (1975). The Rayleigh critical value defines the criterion that must be approximately met or exceeded to achieve convection and is calculated by the equation

$$Ra_c \approx 4\pi^2 \approx 40 \quad (3.3)$$

For verification of liquid convection within the models the Rayleigh number is solved for the high permeability large checkerboard model (Figure 9b) using a permeability of  $10^{-10} \text{ m}^2$  such that

$$\text{Ra} = \frac{(10^{-10} \text{ m}^2)(9.81 \text{ m/s}^2)(2.0 \times 10^{-4} \text{ K}^{-1})(4.0 \times 10^6 \text{ W-s/m}^3 \text{ K})(28 \text{ m})(10 \text{ K})}{(4.0 \times 10^{-7} \text{ m}^2/\text{s})(1.25 \text{ W/mK})}$$

This equates to a Ra value of 439, greatly exceeding the Rayleigh critical value of 40. This provides support to the idea that the liquid in the lower domain of the high permeability models (Figures 8b, 9b and 10b) is convecting.

The convection occurring at the lower model domain of the high permeability simulations (Figures 8b, 9b, and 10b) creates a non-linear temperature profile, different from the temperature profile created solely by conduction in the low permeability simulations (Figures 8a, 9a, and 10a). Both temperature profiles for the homogeneous model can be seen in Figure 14.

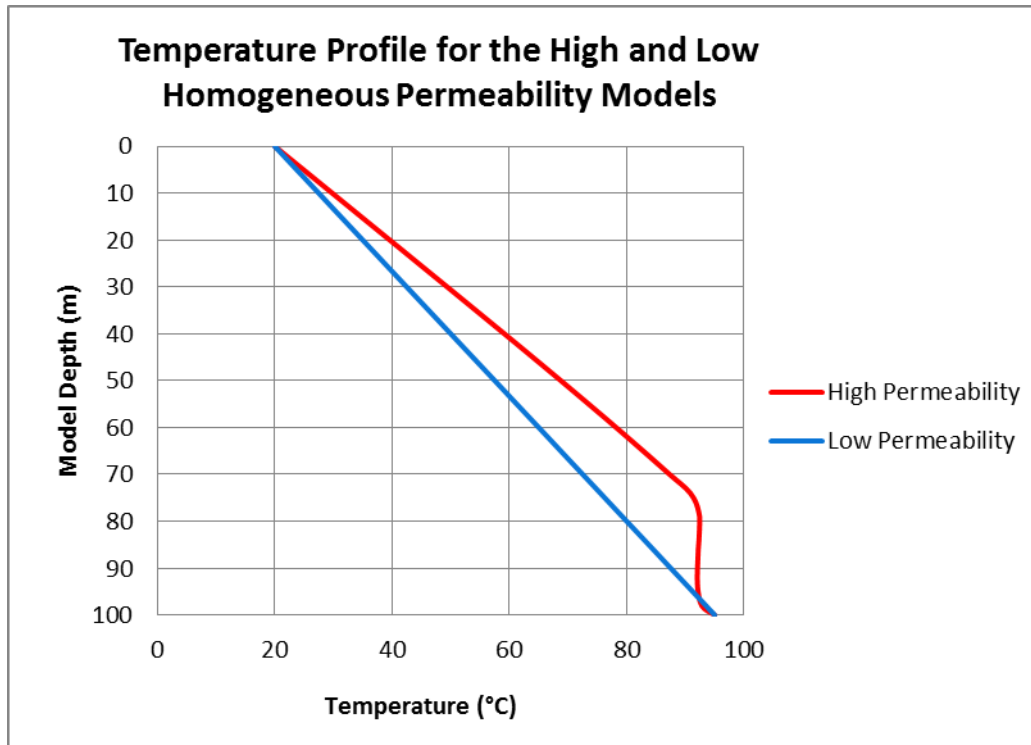


Figure 14: Temperature profile in the center (column 13) of the high and low homogeneous permeability models.

The homogeneous model was chosen to display in Figure 14 because it showed smaller changes in temperature horizontally relative to the heterogeneous models, such that the temperature profile of a single column would be representative of the rest of the model. The non-linear portion of the temperature profile for the homogeneous high permeability model only exists below 70 meters depth in the area saturated with liquid. Above the area saturated with liquid the heat flow is roughly 2 J/s and is transported by conduction to the near surface.

The increase in temperature resulting from an increase in permeability can be best explained by incorporating equation 2.4 into equation 2.5 and rearranging to solve for the vertical temperature gradient, which can be written as

$$\frac{dT}{dz} = \frac{\sum_{\beta} h_{\beta} \left( -k \frac{k_r \beta \rho_{\beta}}{\mu_{\beta}} \left( \frac{dP_{\beta}}{dz} - \rho_{\beta} g \right) \right) - F^{NK+1}}{\lambda} \quad (3.4)$$

where  $\frac{dT}{dz}$  represents the temperature gradient and an increase in the permeability ( $k$ ) results in an increase in this value. Although the spatial variability of increased permeability was able to significantly affect temperature and liquid saturation at depth it was unable to significantly affect the temperature or saturation near the surface.

### 3.2 Thermal Conductivity Results

Changes in thermal conductivity of  $0.5 \text{ Wm}^{-1}\text{K}^{-1}$  and  $3.5 \text{ Wm}^{-1}\text{K}^{-1}$  (low and high thermal conductivity respectively) were tested in three model domains (homogeneous, large checkerboard, and vertical layers) for a total of six simulations outlined in Table 1 as simulations numbers 4, 5, 12, 13, 20, and 21. Of the six model simulations testing thermal conductivity only two had a significant horizontal change in temperature at two meters depth. The large checkerboard model with high altered thermal conductivity (Figure 16b) and low altered thermal conductivity (Figure 16a) showed horizontal changes in temperature at two meters depth of approximately  $0.25 \text{ }^{\circ}\text{C}$  and  $0.8 \text{ }^{\circ}\text{C}$ , respectively. The remaining four models (Figures 15a, 15b, 17a, and 17b) only displayed horizontal variation in temperature at depth where the model was saturated with liquid.

Of the six models testing thermal conductivity the greatest horizontal change in temperature throughout any entire model was 12.4 °C, in the high thermal conductivity large checkerboard model. All thermal conductivity modeling results are shown in Figures 15-17.



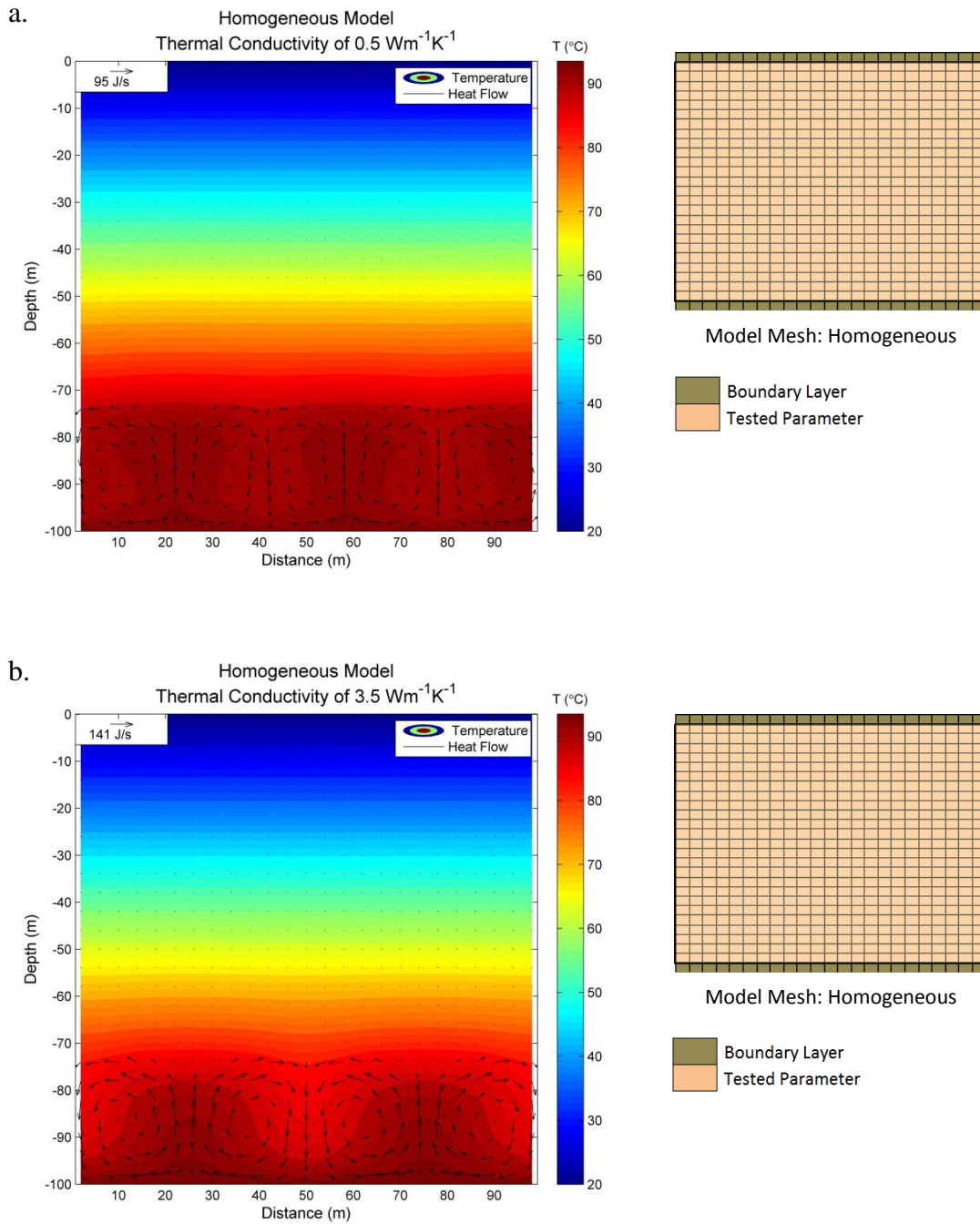


Figure 15: Results of the thermal conductivity simulations in a homogeneous model domain. Colored temperature contours are shown in  $^{\circ}\text{C}$  and are overlain by heat flow vectors. a) Simulation 4 - Low thermal conductivity ( $0.5 \text{ Wm}^{-1}\text{K}^{-1}$ ) with heat flow up to  $95 \text{ J/s}$ ; b) Simulation 5 - High thermal conductivity ( $3.5 \text{ Wm}^{-1}\text{K}^{-1}$ ) with heat flow up to  $141 \text{ J/s}$ .

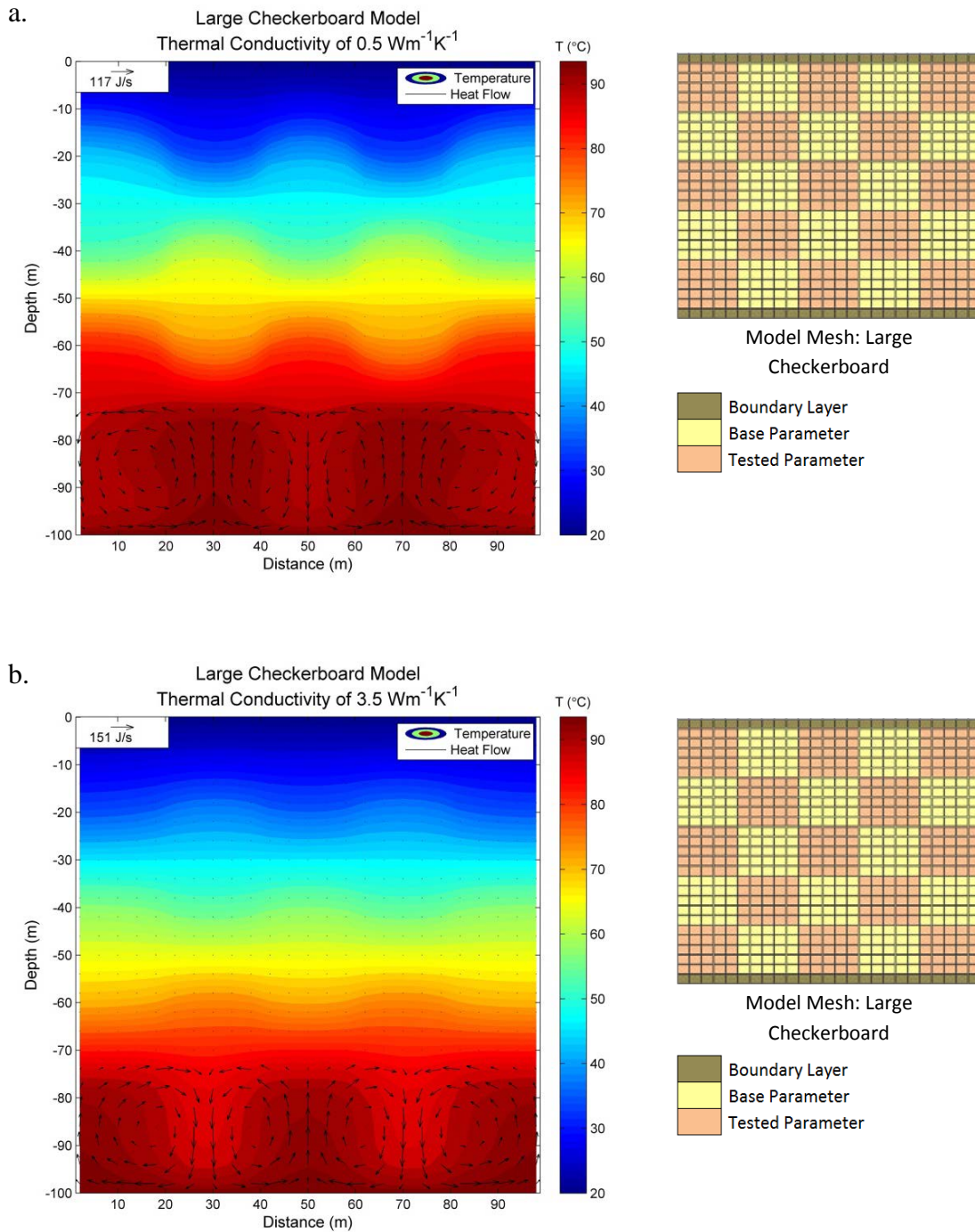


Figure 16: Results of the thermal conductivity simulations in a large checkerboard model domain. Colored temperature contours are shown in  $^{\circ}\text{C}$  and are overlain by heat flow vectors. a) Simulation 12 - Low thermal conductivity ( $0.5 \text{ Wm}^{-1}\text{K}^{-1}$ ) with heat flow up to  $117 \text{ J/s}$ ; b) Simulation 13 - High thermal conductivity ( $3.5 \text{ Wm}^{-1}\text{K}^{-1}$ ) with heat flow up to  $151 \text{ J/s}$ .

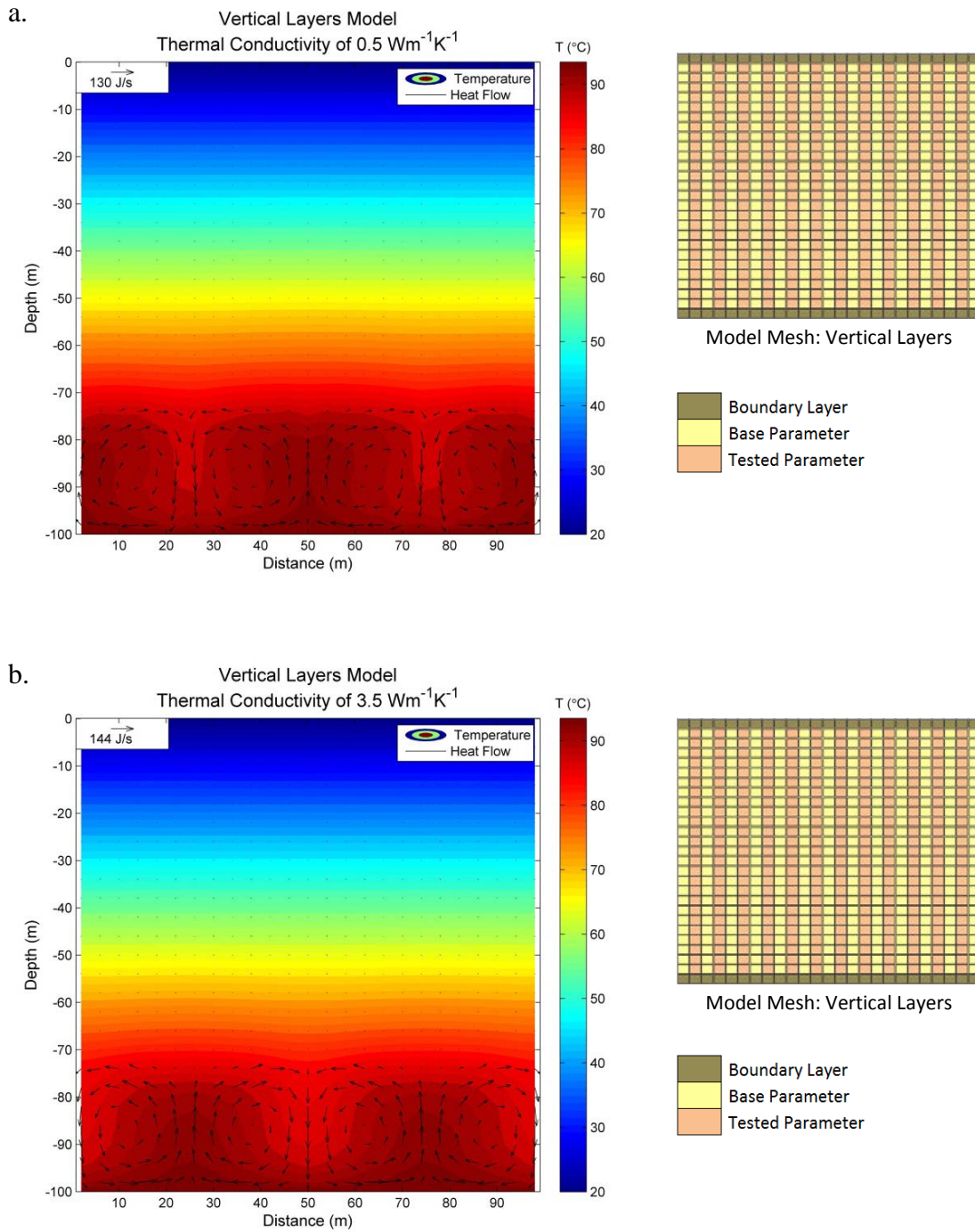


Figure 17: Results of the thermal conductivity simulations in a vertical layers model domain. Colored temperature contours are shown in  $^{\circ}\text{C}$  and are overlain by heat flow vectors. a) Simulation 20 - Low thermal conductivity ( $0.5 \text{ Wm}^{-1}\text{K}^{-1}$ ) with heat flow up to  $130 \text{ J/s}$ ; b) Simulation 21 - High thermal conductivity ( $3.5 \text{ Wm}^{-1}\text{K}^{-1}$ ) with heat flow up to  $144 \text{ J/s}$ .

Figures 15-17 show heat flow circulating in the lower regions of all of the thermal conductivity models, as in the high permeability simulations. This convection in the lower saturated region is possible because the permeability is greater than  $10^{-12} \text{ m}^2$  homogeneously in these models, such that convection is not limited by low permeability. Note that both low and base permeability models essentially have the same amounts of liquid in the lower domain at steady state. Altered thermal conductivity had the most significant effect in the large checkerboard heterogeneity (Figure 16) and the heat flow caused the largest temperature disturbances in the blocks of cells with the higher thermal conductivities. The thermal conductivity did not cause horizontal disturbances in temperature at the near surface in the homogeneous model (Figure 15) due to the parameters being the same throughout the entire model. However, in Figure 17 the thermal conductivity did not have significant temperature disturbances at the near surface due to the thermal conductivity changing too frequently in every other horizontal cell.

In all thermal conductivity modeling simulations the heat flow increases approximately 15-45 J/s with the corresponding increase in the thermal conductivity from  $0.5 \text{ Wm}^{-1}\text{K}^{-1}$  to  $3.5 \text{ Wm}^{-1}\text{K}^{-1}$ , thus supporting that an increase in thermal conductivity would result in an increase in heat flux. This deduction can be further supported by equation 1.1, which is the conductive component of equation 2.5 and written as

$$H = -\lambda \frac{dT}{dz} \quad (3.5)$$

where the negative sign represents the flow of heat from high to low temperatures. An increase in thermal conductivity in all cases will increase heat flux from cell to cell, thus increasing heat flow.

### **3.3 Porosity Results**

Changes in porosity of 0.25 and 0.50 (low and high porosity respectively) were tested in three model domains (homogeneous, large checkerboard, and vertical layers) for a total of six simulations outlined in Table 1 as simulations numbers 6, 7, 14, 15, 22, and 23. Of the six model simulations testing porosity, only one showed a change in temperature at two meters depth. The large checkerboard model with low altered porosity (Figure 19a) showed the greatest horizontal changes in temperature at two meters depth of 0.25 °C. The same model (Figure 19a) also had the greatest horizontal change in temperature throughout any entire model of 6.0 °C. All other remaining porosity simulations showed essentially identical results, displaying the same heat flow patterns and temperature gradients. All porosity modeling results are shown in Figures 18-20.

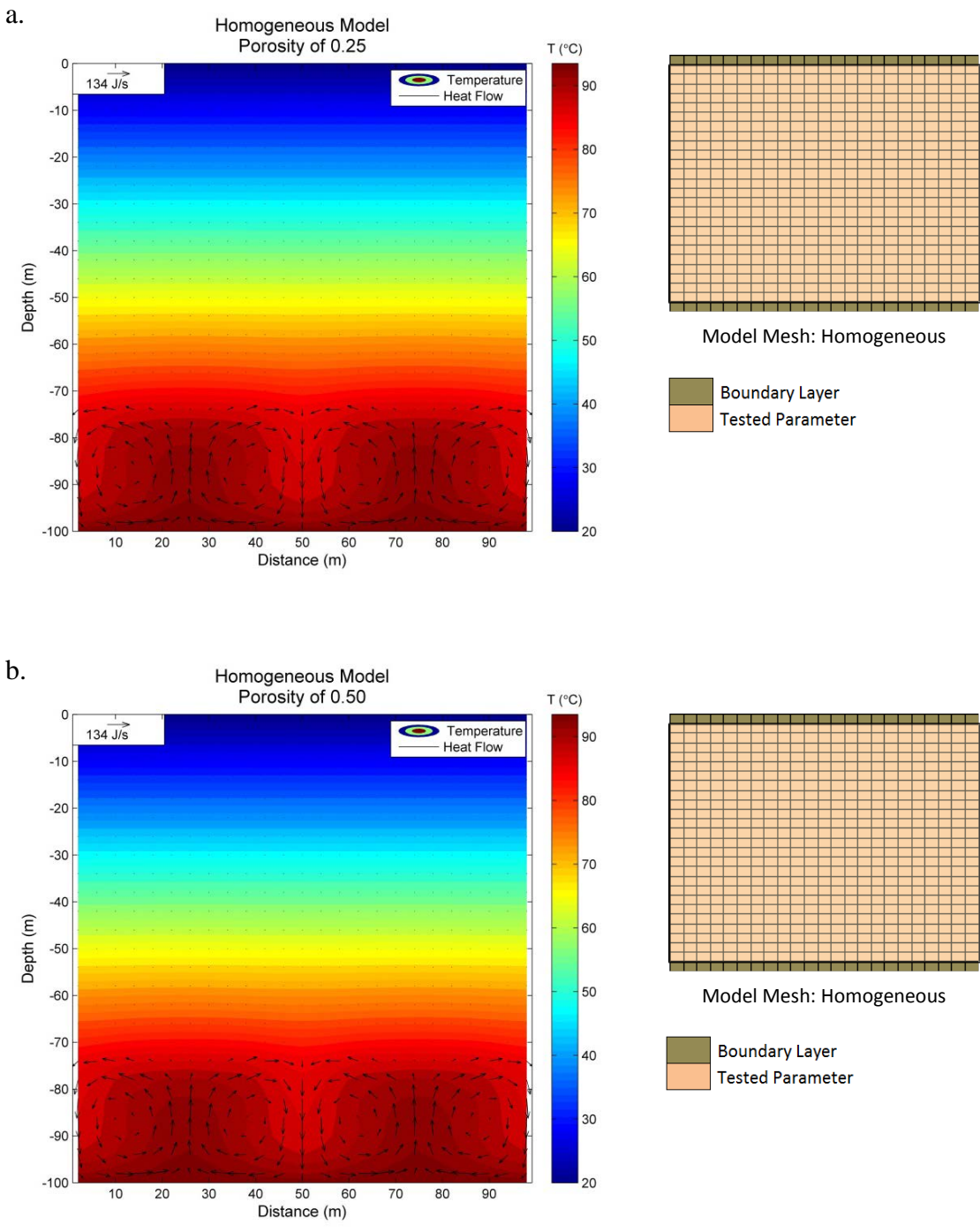


Figure 18: Results of the porosity simulations in a homogeneous model domain. Colored temperature contours are shown in °C and are overlain by heat flow vectors. a) Simulation 6 - Low porosity (0.25) with heat flow up to 134 J/s; b) Simulation 7 - High porosity (0.50) with heat flow up to 134 J/s.

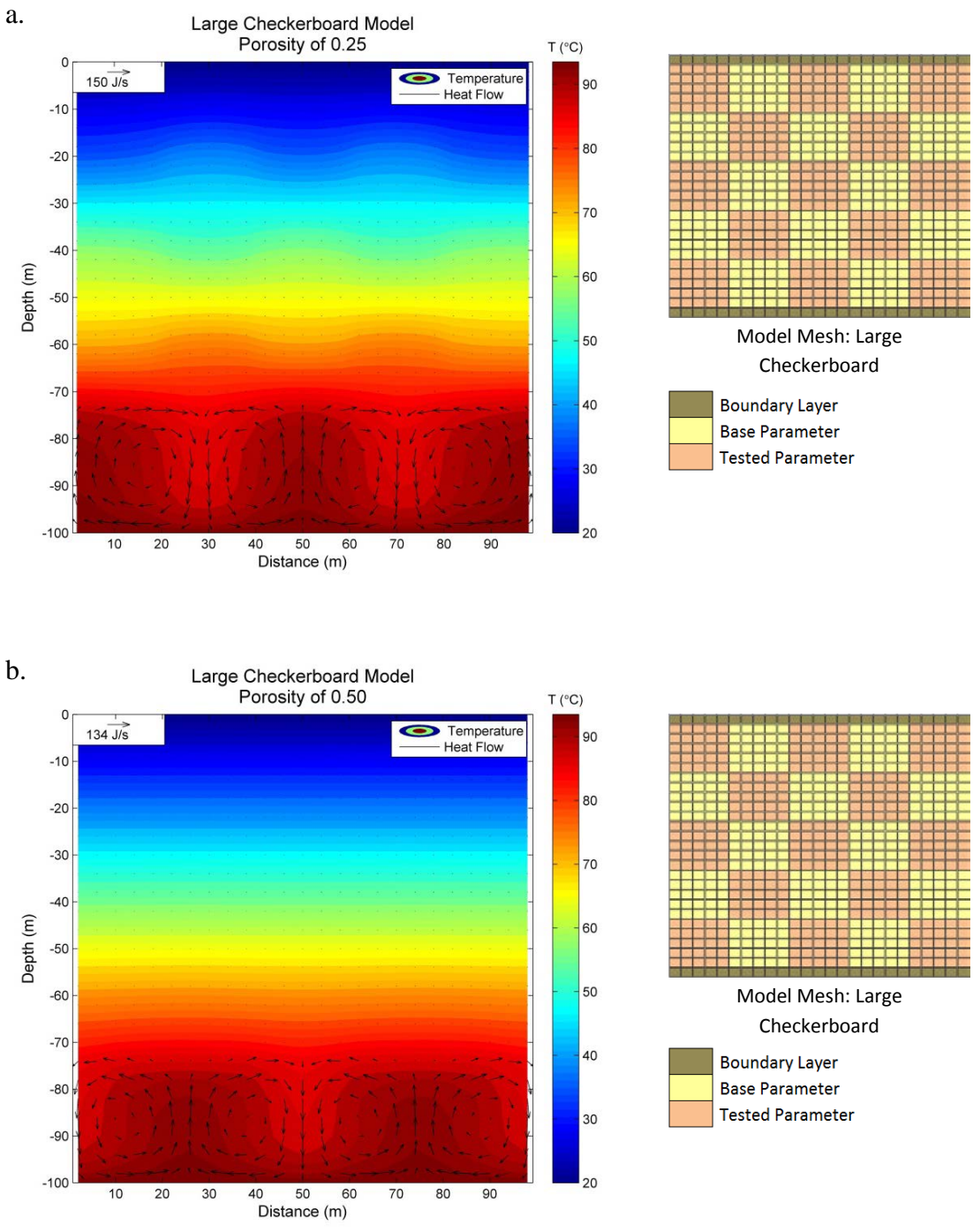


Figure 19: Results of the porosity simulations in a large checkerboard model domain. Colored temperature contours are shown in °C and are overlain by heat flow vectors. a) Simulation 14 - Low porosity (0.25) with heat flow up to 150 J/s; b) Simulation 15 - High porosity (0.50) with heat flow up to 134 J/s.

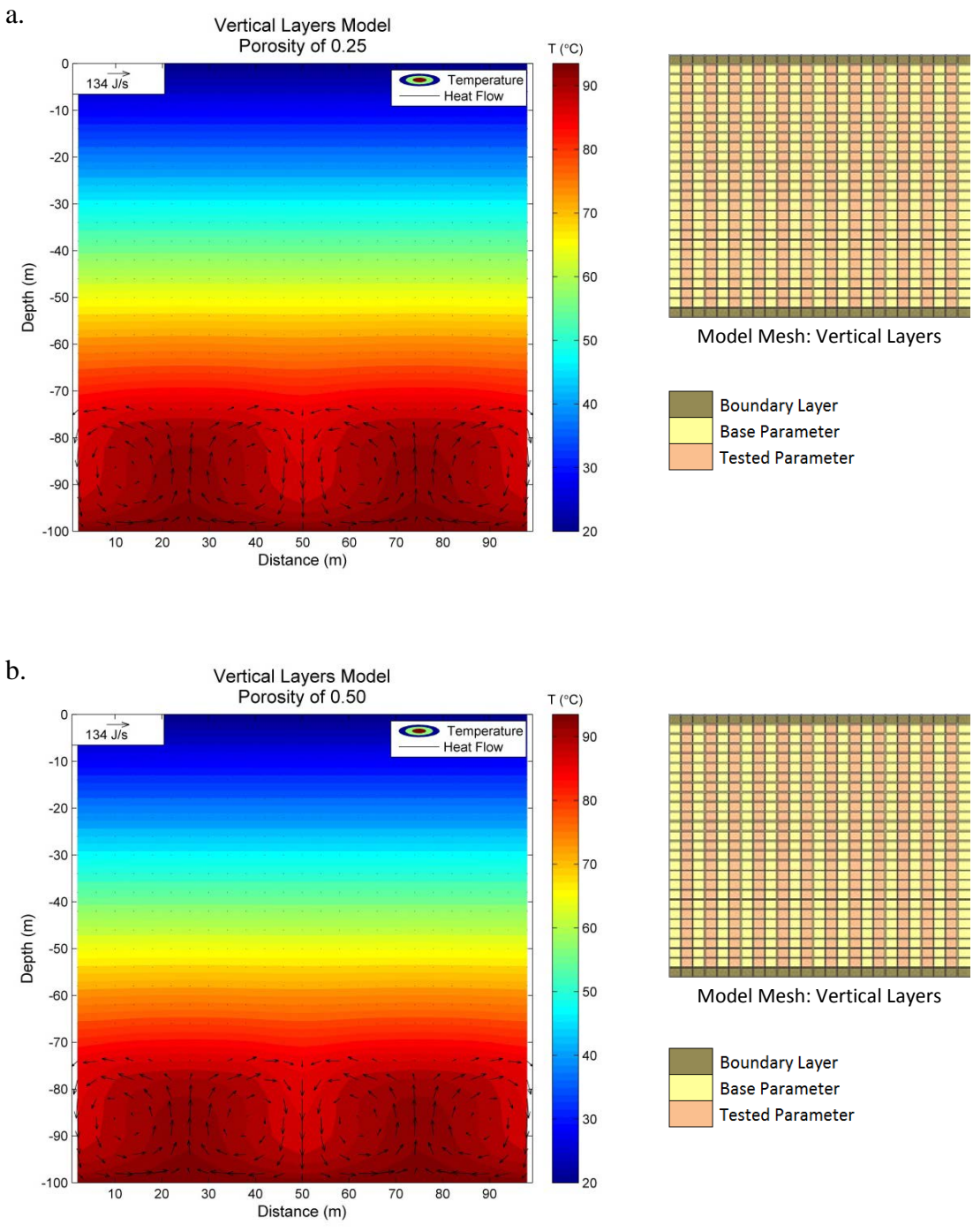


Figure 20: Results of the porosity simulations in a vertical layers model domain. Colored temperature contours are shown in °C and are overlain by heat flow vectors. a) Simulation 22 - Low porosity (0.25) with heat flow up to 134 J/s; b) Simulation 23 - High porosity (0.50) with heat flow up to 134 J/s.



All porosity modeling results excluding the low porosity model in the large checkerboard heterogeneity (Figure 19a) are essentially identical to the base model, showing the same temperature gradient and heat flow pattern. The low porosity, homogeneous model (Figure 18a) is compared to the baseline model in Figure 21.

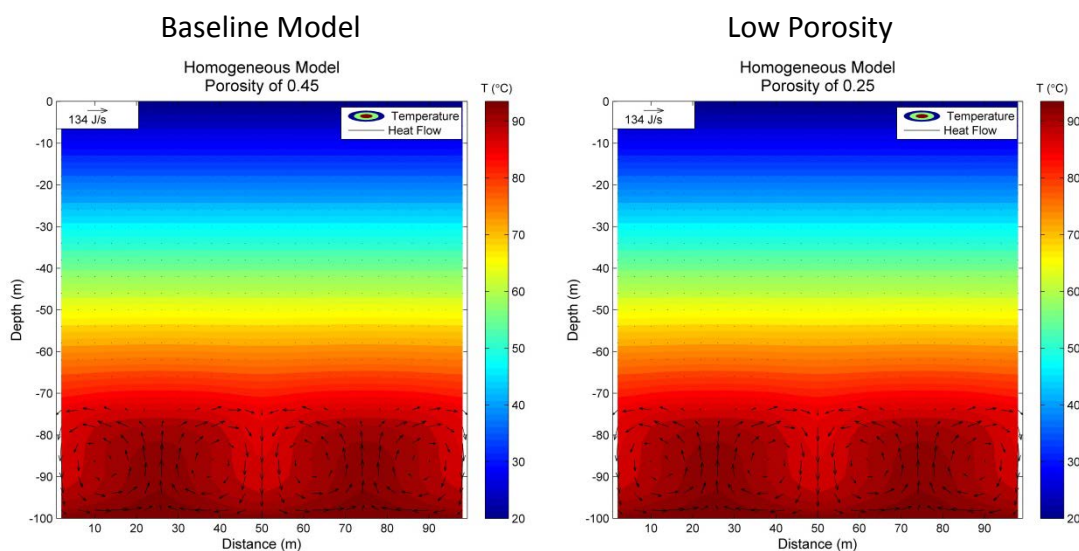


Figure 21: Temperature and heat flow comparison of homogeneous base model (Simulation 1) to the homogeneous, low porosity model (Simulation 6).

These results indicate that porosity changes of 0.20 (0.45 to 0.25, as shown in Figure 21) are not significant enough to affect the heat flow patterns in homogeneous models. Even in the low porosity, vertical layers model the temperature results were identical to the base model, furthermore indicating that for changes in the heat flow patterns to occur with changes of 0.20 porosity or less to occur horizontally, larger heterogeneities are required, such as the large checkerboard heterogeneity.

Baseline porosity was set to 0.45 which is at the higher range of porosity given by Freeze and Cherry (1979) for sand. The difference between baseline porosity of 0.45 and

the high porosity of 0.50 was not significant enough to affect the temperature or heat flow in any of the simulations.

### **3.4 Residual Liquid Saturation Results**

Changes in residual liquid saturation of 0.10 and 0.15 (moderate and high residual liquid saturation respectively) were tested in three model domains (homogeneous, large checkerboard, and vertical layers) for a total of six simulations outlined in Table 1 as simulations numbers 8, 9, 16, 17, 24, and 25. Of the six model simulations testing residual liquid saturation, only two showed significant horizontal changes in temperature at two meters depth. The large checkerboard model with testing high residual liquid saturation showed the most significant horizontal change in temperature at two meters depth of 0.78 °C, followed by the large checkerboard model testing moderate residual liquid saturation, which showed a horizontal change in temperature at two meters depth of 0.24 °C. Of the six models testing residual liquid saturation the greatest horizontal change in temperature throughout any entire model was 9.4 °C, in the high residual liquid saturation large checkerboard model. The results for all of the residual liquid saturation models are shown in Figure 22-24.

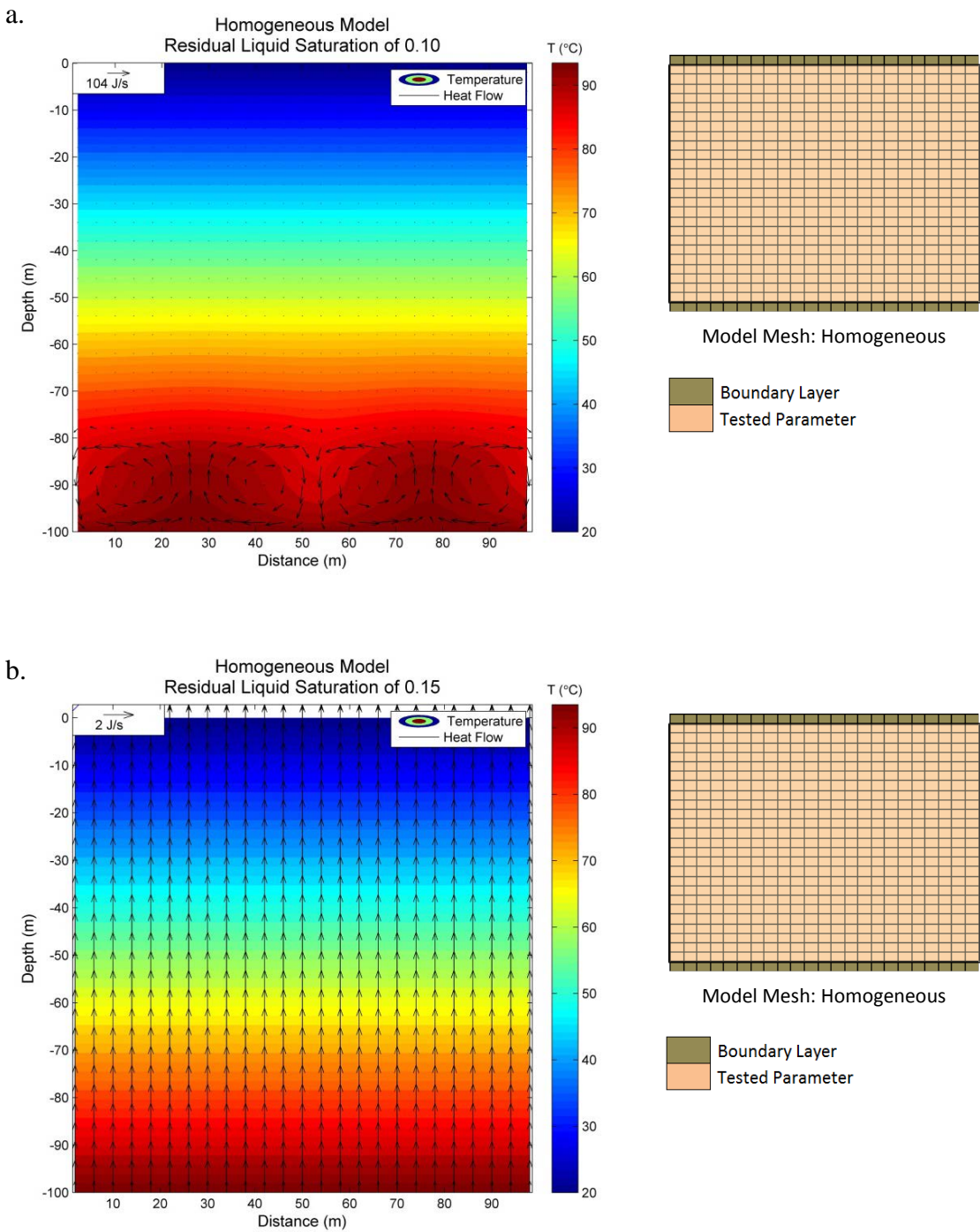


Figure 22: Results of the residual liquid saturation simulations in a homogeneous model domain. Colored temperature contours are shown in °C and are overlain by heat flow vectors. a) Simulation 8 - Moderate residual liquid saturation (0.10) with heat flow up to 104 J/s; b) Simulation 9 - High residual liquid saturation (0.15) with heat flow up to 2 J/s.

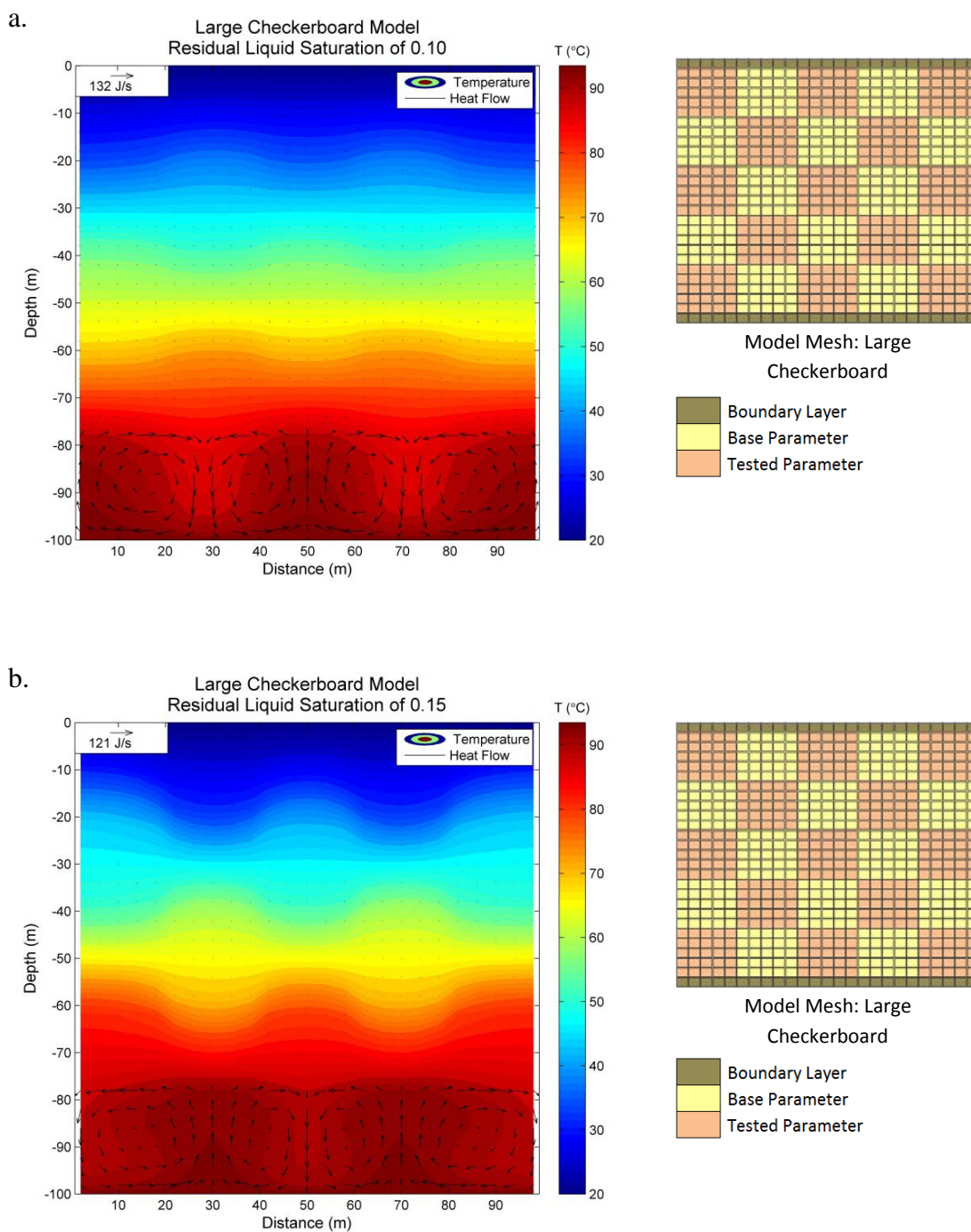


Figure 23: Results of the residual liquid saturation simulations in a large checkerboard model domain. Colored temperature contours are shown in °C and are overlain by heat flow vectors. a) Simulation 16 - Moderate residual liquid saturation (0.10) with heat flow up to 132 J/s; b) Simulation 17 - High residual liquid saturation (0.50) with heat flow up to 121 J/s.

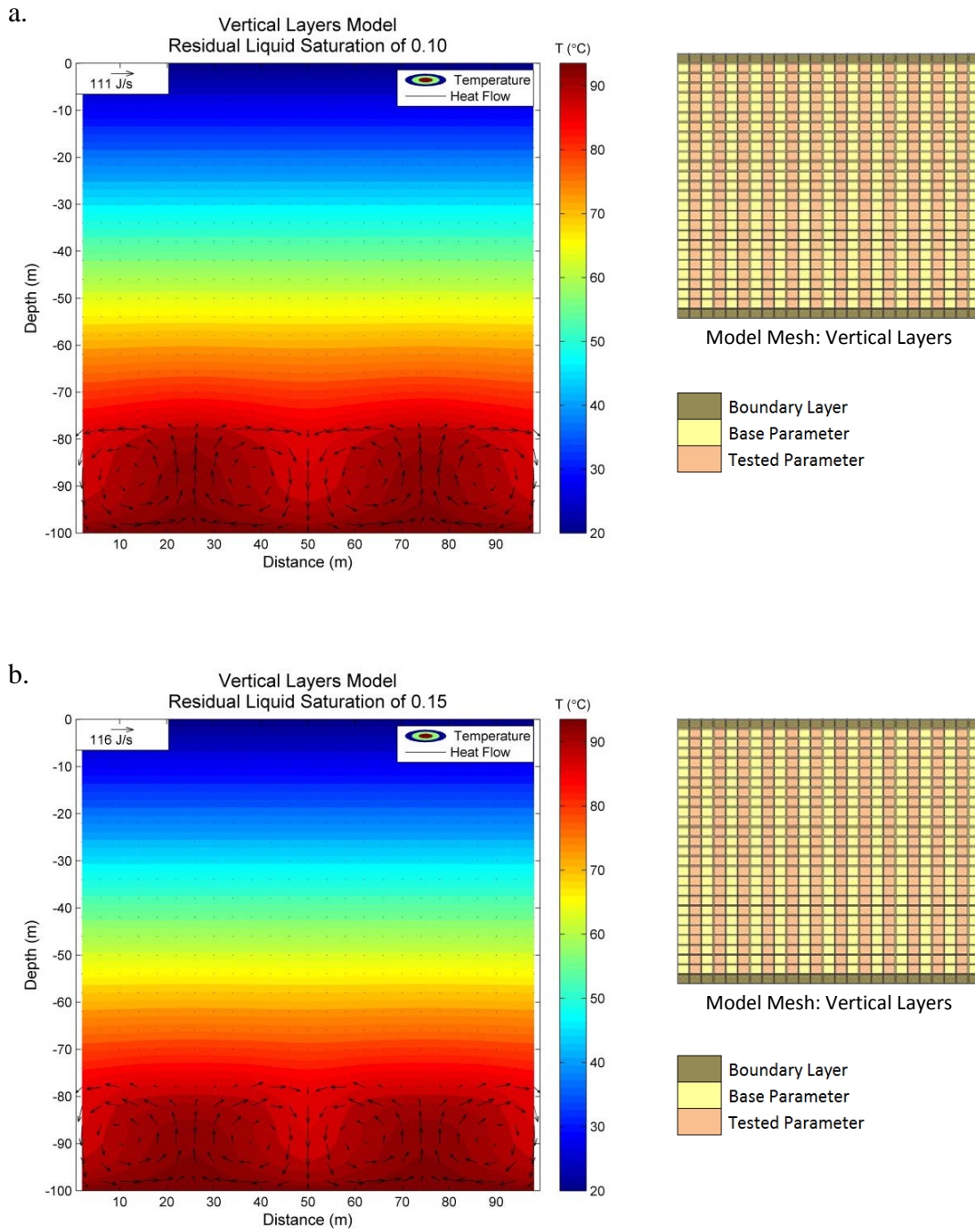


Figure 24: Results of the residual liquid saturation simulations in a vertical layers model domain. Colored temperature contours are shown in °C and are overlain by heat flow vectors. a) Simulation 24 - Moderate residual liquid saturation (0.10) with heat flow up to 111 J/s; b) Simulation 25 - High residual liquid saturation (0.50) with heat flow up to 116 J/s.

In all of the simulations testing increased residual liquid saturation (Figures 22-24) the maximum heat flow did not exceed the maximum heat flow in the base model (base model had a maximum heat flow of 134 J/s); this is due to the residual liquid saturation being increased from 0.045 to 0.10 and 0.15 in these six simulations (simulations 8, 9, 16, 17, 24, and 25 in Table 1). This increase in residual liquid saturation decreases the amount of fluid that can be drained to the lower portion of the model domain. The decreased amount of fluid results in decreased flow and smaller circulating cells of liquid water, which transports the heat. Thus, the increase in residual liquid saturation results in a decrease in heat flow, and changes in residual liquid saturation therefore have the effect of raising or lowering the depth at which heat flow becomes conduction dominated within the model domain. Note that without a partially saturated zone in the lower domain, the heat transport is solely due to conduction at 2 J/s in all models.

In the homogeneous model altered with a high residual liquid saturation (Figure 22b), heat was transported by conduction rather than convection, unlike the other residual liquid saturation models. The increased residual saturation of all 625 grid cells to 0.15 resulted in a decreased saturation of less than 0.9 in the lower model domain. The liquid saturation of the homogeneous, residual liquid saturation model is shown in comparison to the base model in Figure 25 overlaid by heat flow vectors.

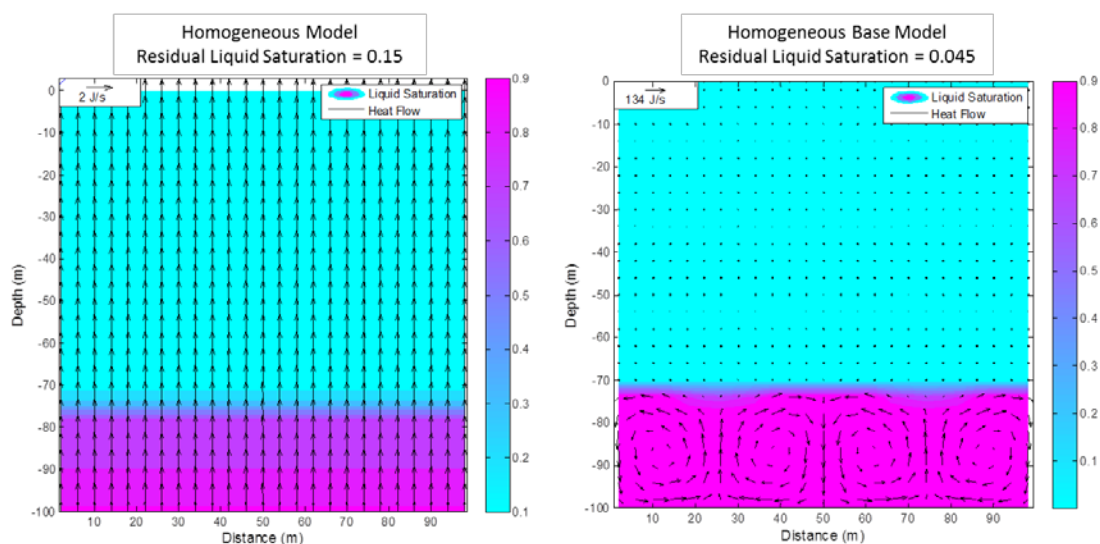


Figure 25: Heat flow vectors overlaying a liquid saturation plot for the homogeneous model with high residual liquid saturation (Simulation 9) in comparison to the base model (Simulation 1).

In the homogeneous, high residual liquid saturation model the water table remains at the lower boundary layer and does not fully saturate and rise as the fluid drained. The highest liquid saturation in the inner 625 cells of this model is approximately 0.84. This lack of liquid saturation in the lower model domain is what causes the heat flow to be transported by conduction rather than convection. It is this model that has the lowest temperature at two meters depth.

Both vertical layer models and the homogeneous model with moderate residual liquid saturation exhibit the same heat flow pattern as the base model, but all show decreased maximum heat flow relative to the base model ranging from 104-116 J/s.

### 3.5 Additional Modeling Results

Additional modeling testing a low and high thermal conductivity with an increased isolated temperature in a large checkerboard heterogeneity (Simulations 26 and 27) produced some interesting results. These two models were essentially the same as Simulations 12 and 13, therefore the results are fairly similar and comparable to Figures 16a and 16b. The results for Simulations 26 and 27 are shown in Figure 26.

Figure 26a and 26b show the same pattern of heat flowing up through areas of higher thermal conductivity and down through areas of lower conductivity that is seen in Figures 16a and 16b (same model without an increased isolated temperature). However, Figure 26a shows less maximum heat flow than Figure 16a (111 J/s compared to 117 J/s, respectively), while Figure 26b shows a greater maximum heat flow than Figure 16b (213 J/s compared to 151 J/s, respectively). The increased isolated temperature model with testing low thermal conductivity showed a horizontal change in temperature of 0.8 °C, while the increased isolated temperature model testing high thermal conductivity showed a horizontal change in temperature of 0.26 °C - this is very similar to what is seen in Figures 16a and 16b. However, the greatest horizontal change in temperature throughout the entire model domain in Figures 26a and 26b is less than what is shown in Figure 16a and 16b. The low thermal conductivity model with increased isolated temperature (Figure 26a) showed a maximum horizontal change in temperature throughout the entire model of 9.7 °C, while the high thermal conductivity model with increased isolated temperature (Figure 26b) showed a maximum horizontal change in temperature throughout the entire model of 7.0 °C.



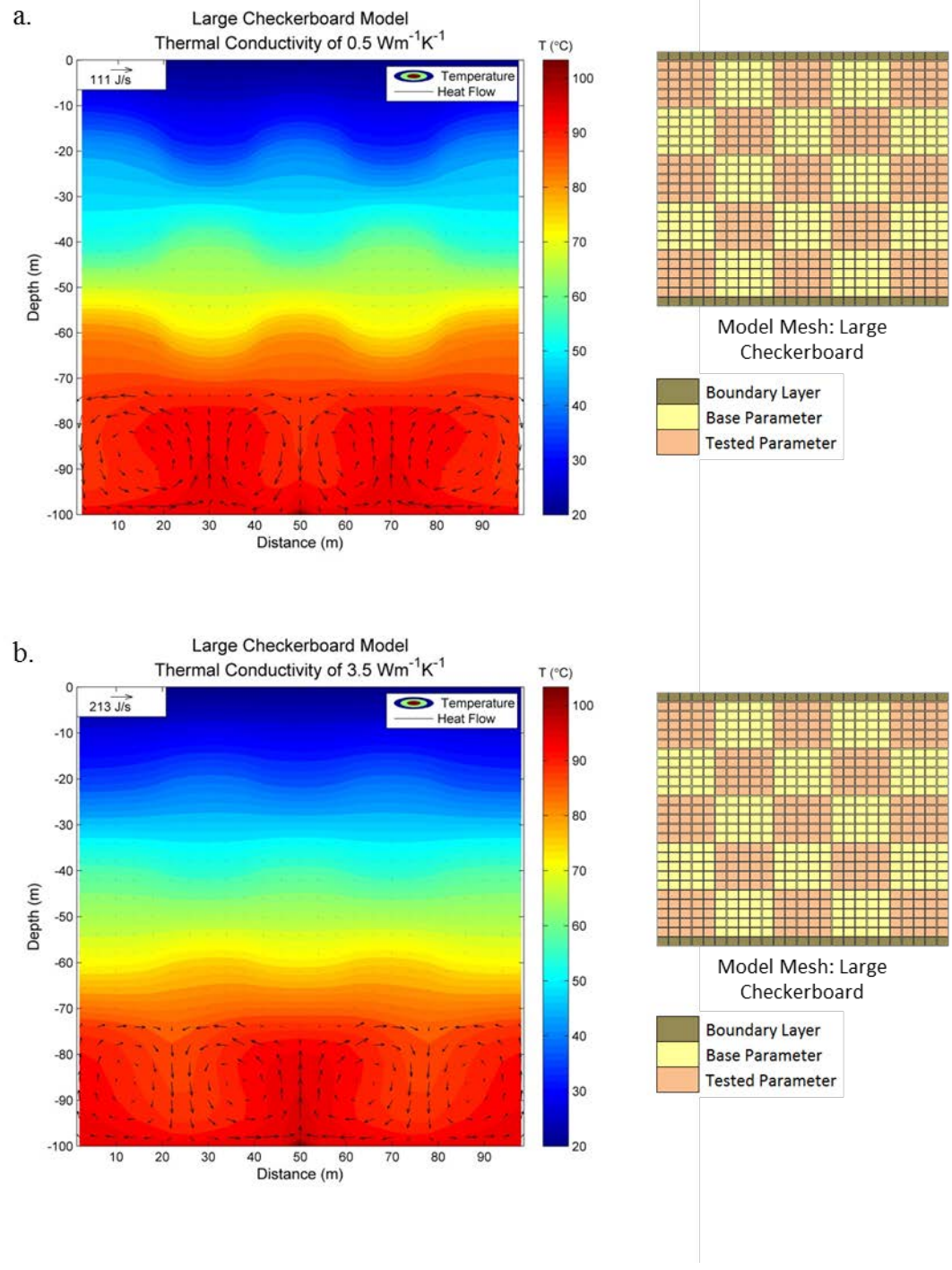


Figure 26: Results of the thermal conductivity simulations with an isolated increased temperature in a large checkerboard model domain. Colored temperature contours are shown in °C and are overlain by heat flow vectors. a) Simulation 26 - Low thermal conductivity ( $0.5 \text{ Wm}^{-1}\text{K}^{-1}$ ) with heat flow up to 111 J/s; b) Simulation 27 - High thermal conductivity ( $3.5 \text{ Wm}^{-1}\text{K}^{-1}$ ) with heat flow up to 213 J/s.

Additional modeling testing a low and high thermal conductivity in a smaller vertical domain with a large checkerboard heterogeneity (Simulations 28 and 29, respectively) produced the expected results. Simulation 28 (low thermal conductivity) showed horizontal changes in temperature of up to 1.7 °C, while Simulation 29 (high thermal conductivity) showed horizontal changes in temperature of 0.53 °C, both greater than that of the corresponding 100m vertical domain models (Simulations 12 and 13). While both simulations showed a greater horizontal change in temperature at two meters depth than the 100 m vertical domain models, only the low thermal conductivity model (Simulation 28) had a greater horizontal change in temperature throughout the entire model domain of 21°C compared to 9.8 °C in the corresponding simulation with a 100 m vertical domain (Simulation 12). Meanwhile, the high thermal conductivity model (Simulation 29) had a lower horizontal change in temperature throughout the entire model domain than the corresponding 100 m vertical domain model (Simulation 13) – 9.1 °C and 12.5 °C, respectively. The results for Simulations 28 and 29 are shown in Figure 27.

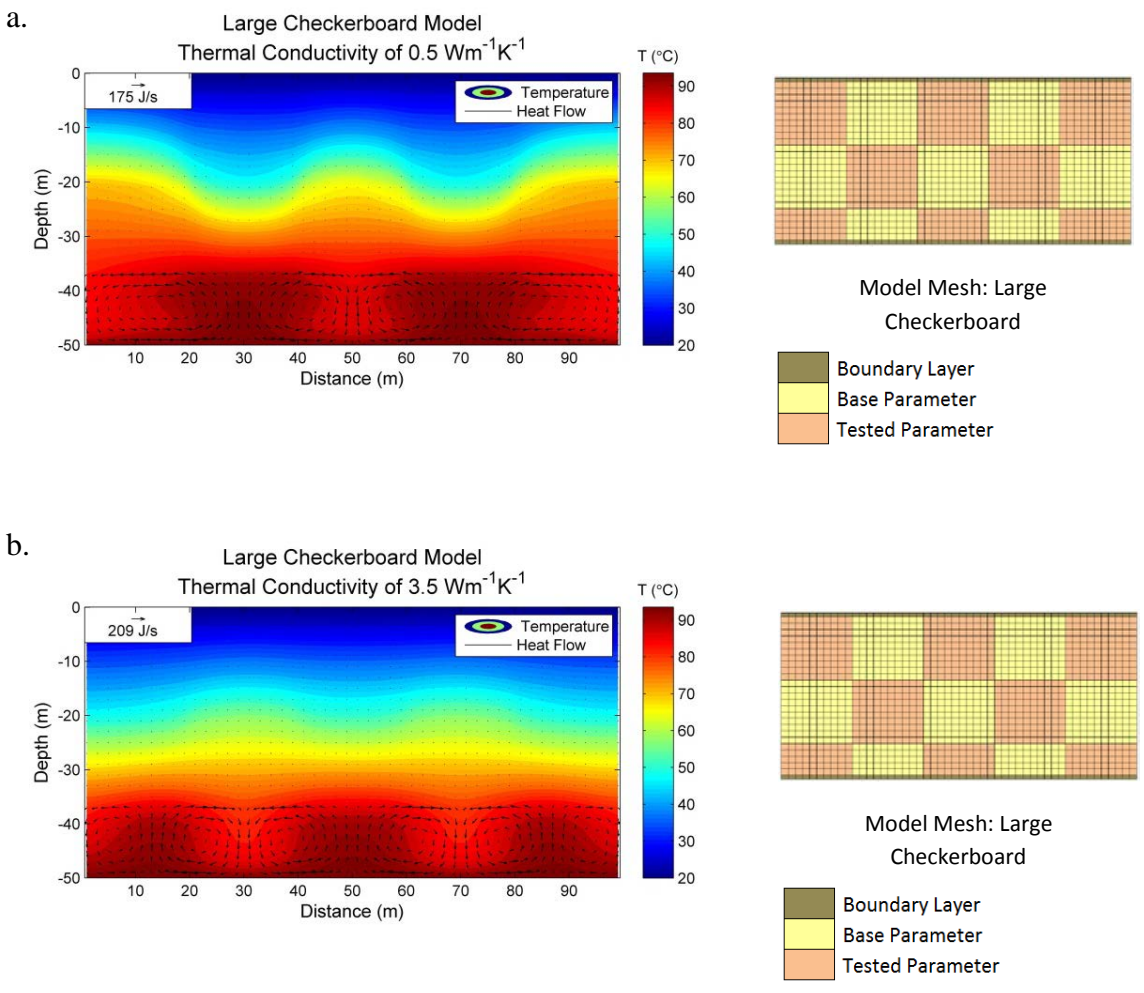


Figure 27: Results of the thermal conductivity simulations with an isolated increased temperature in a large checkerboard model domain. Colored temperature contours are shown in °C and are overlain by heat flow vectors. a) Simulation 26 - Low thermal conductivity ( $0.5 \text{ Wm}^{-1}\text{K}^{-1}$ ) with heat flow up to 111 J/s; b) Simulation 27 - High thermal conductivity ( $3.5 \text{ Wm}^{-1}\text{K}^{-1}$ ) with heat flow up to 213 J/s.

## CHAPTER 4

### DISCUSSION

#### 4.1 Comparisons of Parameters Tested

The maximum horizontal changes in temperature at two meters depth for all 24 initial simulations are shown in Table 2. Note that while 25 simulations were run initially, this table does not include the base model.

Approximate Maximum Change in Temperature at Two Meters Depth								
	Permeability		Thermal Conductivity		Porosity		Residual Liquid Saturation	
	$10^{-12} \text{ m}^2$	$10^{-10} \text{ m}^2$	$0.5 \text{ Wm}^{-1}\text{K}^{-1}$	$3.5 \text{ Wm}^{-1}\text{K}^{-1}$	0.25	0.50	0.10	0.15
<b>Homogeneous</b>	0	<0.01	<0.01	0	0	0	0	0
<b>Large Checkerboard</b>	0	<0.01	0.8	0.25	0.25	0	0.24	0.78
<b>Vertical Layers</b>	0	<0.01	<0.01	0	0	0	<0.01	0

Table 2: Approximate changes in temperature ( $^{\circ}\text{C}$ ) at two meters depth for the 24 initial simulations.

Out of the 24 initial simulations shown in Table 2, the largest horizontal change in temperature at two meters depth was  $0.8^{\circ}\text{C}$ , in the model with low thermal conductivity in a large checkerboard pattern. For this study, thermal conductivity ranging from  $0.5 \text{ Wm}^{-1}\text{K}^{-1}$  to  $3.5 \text{ Wm}^{-1}\text{K}^{-1}$  was tested, however thermal conductivities for sand have been measured to reach as high as  $4.3 \text{ Wm}^{-1}\text{K}^{-1}$  (Raznjevic, 1976), meaning that the horizontal change in temperature could be even greater (i.e., exceeding  $1^{\circ}\text{C}$ ) at two meters depth or even throughout the entire model in heterogeneous situations where the thermal conductivity of a sand varies.

The maximum horizontal changes in temperature throughout the entire model domain for the 24 initial simulations are shown in Table 3. Again, note that although 25 simulations were initially run, the base model is not detailed in this table.

Approximate Maximum Horizontal Change in Temperature								
	Permeability		Thermal Conductivity		Porosity		Residual Liquid Saturation	
	$10^{-12} \text{ m}^2$	$10^{-10} \text{ m}^2$	$0.5 \text{ Wm}^{-1}\text{K}^{-1}$	$3.5 \text{ Wm}^{-1}\text{K}^{-1}$	0.25	0.50	0.10	0.15
<b>Homogeneous</b>	0.0	2.6	2.9	6.3	5.3	5.4	5.4	0.0
<b>Large Checkerboard</b>	0.0	4.2	9.8	12.5	6.0	5.4	5.8	9.4
<b>Vertical Layers</b>	0.0	2.5	4.8	6.0	5.4	5.4	5.3	5.3

Table 3: Approximate changes in temperature ( $^{\circ}\text{C}$ ) throughout the entire model for 24 initial simulations.

Out of the 24 initial simulations detailed here, the largest horizontal change in temperature throughout the entire model domain (at any depth in the model) was  $12.5^{\circ}\text{C}$ , in the model with high thermal conductivity in a large checkerboard pattern. Both maximum horizontal change in temperature at two meters depth and throughout the entire model have their highest change in the large checkerboard model with changes in thermal conductivity, although at two meters depth the greatest horizontal change in temperature occurred as a result of changes to low ( $0.5 \text{ Wm}^{-1}\text{K}^{-1}$ ) thermal conductivity and in the entire model the greatest horizontal change in temperature occurred as a result of changes to high ( $3.5 \text{ Wm}^{-1}\text{K}^{-1}$ ) thermal conductivity. The horizontal change in temperature increased significantly in the center region of the model compared to two meters depth.

Of all the parameters tested, changes in permeability caused the least horizontal change in temperature at any depth in the model. However, the high permeability models had maximum heat flows ranging from 494-741 J/s, 343 J/s greater than any of the other

models. Additionally, permeability was the only parameter tested that showed a change in all models in the heat transport method between the high and low values tested. That is, in changing permeability from  $10^{-11} \text{ m}^2$  to  $10^{-12} \text{ m}^2$  resulted in a change in the heat transport method from convection to solely conduction. This indicates that there is a critical value between  $10^{-11} \text{ m}^2$  and  $10^{-12} \text{ m}^2$  at which liquid flow becomes limited and can no longer circulate, due to the decreased ability of the rock to transmit fluid.

The only other conduction dominated model is the homogeneous, high residual liquid saturation model shown in Figure 22b. Interestingly, the temperature profile in this model was the same as the temperature profile in the low permeability models. In this case the absence of convection is due to the lack of saturation, unlike the low permeability cases where it was due to decreased fluid flow.

Of all the parameters tested porosity showed the least significant impact on the heat flow from the deeper geothermal reservoir to the near surface. The temperature profile and heat flow in five of the six porosity models were identical to that of the base model.

The additional modeling of thermal conductivity in a large checkerboard heterogeneity with increased isolated temperature (Simulations 26 and 27) produced similar heat flow patterns to the models without the increased isolated temperature (Simulations 12 and 13), which might be expected. However the increased isolated temperature did not amplify the horizontal disturbance in temperature which is not what might be expected, as shown in the conceptual image Figure 2.

Shortening the vertical domain created the largest horizontal change in temperature at two meters depth and throughout the entire model domain in the low thermal conductivity model (Simulation 28). While the high thermal conductivity model (Simulation 29) did not show a greater horizontal change in temperature at depth relative to the corresponding 100 m vertical domain model (Simulation 13), the increased horizontal change at two meters depth for both 50 m vertical domain models (Simulations 28 and 29) indicates that a shallower geothermal heat source will have a greater effect on variations in temperature at shallow depths.

#### **4.2 Comparison to Related Work**

The study by Olmsted and Ingebritsen (1986) at the Upsal Hogback geothermal area found that areal changes in thermal diffusivity could lead to changes in temperature at 2 meters depth of up to 4 °C that are unrelated to increased temperature at depth. Thermal diffusivity is directly related to thermal conductivity (a parameter in this study) and is expressed by equation below (Carslaw and Jaeger, 1959).

$$D = \frac{\lambda}{\rho C_p}$$

where  $D$  is thermal diffusivity,  $\lambda$  is thermal conductivity of the rock or fluid,  $\rho$  is density of the rock or fluid, and  $C_p$  is specific heat capacity of the rock or fluid.

Thermal diffusivity is directly related to thermal conductivity allowing the comparison of the results presented in this study to theirs. The study presented here showed changes of up to 0.8 °C in temperature at two meters depth, which is less than

what the study by Olmsted and Ingebritsen found. The varying degree of thermal diffusivity at the Upsal Hogback geothermal area is possibly greater than the equivalent range of thermal conductivity tested here as it was only representative of sand, while the Upsal Hogback area could have more than one sediment/rock type. Another factor is the thermal diffusivity at the Upsal Hogback area likely exhibits a less organized heterogeneity than the heterogeneities tested in the study presented here.

Additional data provided by Chris Sladek for Desert Peak, Nevada, where there are several different sediment/rock types at the edge of a geothermal anomaly provided further insight into the relationship with thermal diffusivity. The availability of annual data allowed them to calculate thermal diffusivity using the annual cycle. They found that thermal diffusivity did not show a strong correlation with temperature and that at Desert Peak the temperatures at two meters were likely more affected by other factors that have a strong influence on the surface such as albedo, slope, and vegetation. The correlation between shallow temperatures and thermal diffusivity is likely site dependent and depends on the degree of heterogeneity within the sediment/rock.

#### **4.3 Modeling Limitations and Realistic Expectations**

For the purposes of this study a constant temperature at the upper boundary was required to test the parameters. While the model could have been set with an outflow of heat flux at the upper boundary, this was not possible given the parameters' relationship with heat flux through the model domain, such that it would be impossible to determine



the magnitude of heat flux at the surface. With the temperature at the upper and lower boundary held constant the model is able to create a temperature profile within the inner model which can only be altered by non-vertical heat flow patterns. Realistically, the temperature at the surface is not constant and can be altered by many factors including the presence of an increased geothermal heat flux (Olmsted and Ingebritsen, 1986). However, if the temperature at the upper boundary is not held constant the upper boundary eventually reaches 95 °C, thus eliminating any geothermal gradient. Therefore, when modeling under these conditions a constant temperature must be applied to both the upper and lower boundaries.

Because the surface temperature was not allowed to vary, it had an unrealistic damping effect on horizontal variations in temperature at two meters depth. The maximum horizontal temperature changes in temperature throughout the entire model domains (shown in Table 3) are more likely similar to what would occur in the real world, although there would be some dampening due to atmospheric temperature and the heterogeneities would be less organized. However, although the temperature variations depicted are not entirely realistic, they do give insight into the parameters that would control temperature variations.

#### **4.4 Future Work**

This research tested the impacts of four parameters on temperature at two meters depth and heat flow in a homogeneous model and two heterogeneous models. While these results proved to be very informative, further testing of other heterogeneous patterns could lend insight into the effect of heterogeneities on heat flow. One might want

to test how smaller or even larger checkerboard heterogeneities can affect temperature at two meters depth and heat flow. The checkerboard represents a very general heterogeneity and further testing could find at what smaller size of the checkerboard heterogeneity is there no longer the development of preferential flow paths, thus making the model essentially homogeneous. Additionally the testing of more realistic geological and structural heterogeneities could provide insight into how more realistic heterogeneities can affect the relationship between temperature at two meters and temperature at a greater depth.

For future studies there are multiple ways the model domain could be improved. The lateral boundaries are no flow boundaries so the width of the model domain can often impact the flow patterns of the inner model. One example of this is the homogeneous, high permeability model in which a non-symmetrical flow pattern develops, possibly due to the lack of model width to support the circulatory heat patterns the model attempts to achieve.

The model domain's depth of two meters is in the center of the second row of cells. As described earlier TOUGH2 has a limitation in that the impact of the upper boundary on the geothermal gradient cannot be lessened. One suggestion that could possibly lessen the impact of the upper boundaries constant temperature at two meters depth would be to increase the number of cells vertically, thus increasing the number of cells between two meters and the upper boundary.

## CHAPTER 5

### CONCLUSION

#### 5.1 General Conclusions

The objective of this study was to get a better understanding of the correlation between temperatures at two meters and temperatures at a greater depth (>100 m) in the vadose zone. This study tested 29 different modeling scenarios to determine under what conditions two-meter temperature measurements would not be representative of the temperature at greater depth.

Modeling in vadose zone conditions produced some interesting results. One of those was the liquid saturation and heat flow results for the homogeneous, high residual liquid saturation model, shown in Figure 25. These results indicate that a lack of liquid saturation (vadose zone conditions) results in a linear conductive geothermal gradient under these conditions. Therefore, under these conditions groundwater is the primary conduit for increased and non-linear heat flow.

The results of this study revealed that the temperature at two meters depth could change up to 0.8 °C horizontally with a uniform heat source at the lower boundary. This horizontal change at 2 meters depth is likely less than might be expected in the real world due to the increased effect of the upper boundary by holding the temperature constant. The actual change in temperature that might be expected is likely a value between the maximum change in temperature at two meters depth and the maximum change in temperature found throughout the entire model in this study, as it was further from the

upper boundary effects. The results of this study indicate that the heterogeneous variability of the parameters tested is not enough to horizontally alter temperature at two meters to create the illusion of an increased temperature at depth. Therefore, under the conditions tested in this study the temperature at two meters depth is representative of the temperature at a greater depth, thus further supporting two-meter temperature measurements as a valid tool for geothermal exploration.

## REFERENCES

- Blodgett, L., & Stack, K. (Eds.). (2009). Geothermal 101: Basics of geothermal energy production and use. Geothermal Energy Association. [Online] Available at [http://smu.edu/smunews/geothermal/Geo101\\_final\\_Feb\\_15.pdf](http://smu.edu/smunews/geothermal/Geo101_final_Feb_15.pdf)
- Bloomfield, K.K., Moore, J.N., R.N. Neilson, R.N. (2003). Geothermal energy reduces greenhouse gases. *Geothermal Resources Council Bulletin*, 32, 77-79.
- Bodvarsson, G., Pruess, K., & Lippmann, M. (1986). Modeling of geothermal systems. *Journal of Petroleum Technology*, 38(09), 1-007.
- Carslaw, H. S., & Jaeger, J. C. (1959). *Conduction of Heat in Solids*. Oxford: Clarendon Press, 1959, 2nd ed.
- Chandrasekharam, D., & Bundschuh, J. (Eds.) (2008). *Low-Enthalpy Geothermal Resources for Power Generation*. Leiden: CRC Press.
- Cheng, P. (1978). Heat transfer in geothermal systems. *Advances in Heat Transfer*, 14, 1-60.
- Combarrous, M.A., and Bories, S.A. (1975). Hydrothermal convection in saturated porous media. *Advances in Hydroscience* 10, 231-306. Academic Press, N.Y.
- Coolbaugh, M. F., Sladek, C., Faulds, J. E., Zehner, R. E., & Oppliger, G. L. (2007). Use of rapid temperature measurements at a 2-meter depth to augment deeper temperature gradient drilling. In Thirty-Second Workshop on Geothermal Reservoir Engineering.
- Demirbas, A. (2009). Global renewable energy projections. *Energy Sources, Part B*, 4(2), 212-224.
- Dickson, M. H., & Fanelli, M. (2013). *Geothermal Energy: Utilization and Technology*. Routledge.
- Domenico, P. A., & Schwartz, F. W. (1990). *Physical and Chemical Hydrogeology*. New York: Wiley.
- Fossoul, F., Orban, P., & Dassargues, A. (2011). Numerical simulation of heat transfer associated with low enthalpy geothermal pumping in an alluvial aquifer. *Geologica Belgica*, 14.
- Freeze, R. A., & Cherry, J. (1979). *Groundwater*. Prentice-Hall, Inc Englewood Cliffs, New Jersey, p 604.
- Glassley, W. E. (2010). *Geothermal Energy: Renewable Energy and the Environment*. CRC Press.
- Hart, S. R., Glassley, W. E., & Karig, D. E. (1972). Basalts and sea floor spreading behind the Mariana island arc. *Earth and Planetary Science Letters*, 15(1), 12-18.
- Kanoglu, M., & Bolatturk, A. (2008). Performance and parametric investigation of a binary geothermal power plant by exergy. *Renewable Energy*, 33(11), 2366-2374.
- Kresic, N. (2006). *Hydrogeology and Groundwater Modeling*. CRC press.
- LeSchack, L. A., & Lewis, J. E. (1983). Geothermal prospecting with Shallo-Temp surveys. *Geophysics*, 48(7), 975-996.
- Naterer, G. F. (2002). *Heat Transfer in Single and Multiphase Systems*. CRC Press.
- Olmsted, F. H. (1977). Use of temperature surveys at a depth of 1 meter in geothermal exploration in Nevada. *US, Geol. Surv., Prof. Pap.:(United States),1044*.

- Olmsted, F. H., & Ingebritsen, S. E. (1986). Shallow subsurface temperature surveys in the basin and range province—II. Ground temperatures in the Upsal Hogback geothermal area, West-Central Nevada, USA. *Geothermics*, 15(3), 267-275.
- Pruess, K., Oldenburg, C. and Moridis, G., 1999. TOUGH2 user's guide, version 2.0. Report LBNL-43134, Lawrence Berkeley National Laboratory, Berkeley, Calif.
- Raznjevic, K. (1976). *Handbook of Thermodynamic Tables and Charts*. New York: McGraw-Hill.
- Reeves, D. M., Pohl, G., Lyles, B., Faulds, J., Louie, J., Ehni, B., Kratt, C., Cooper, C., Parashar, R., Pullammanappallil, S., Noel, D. (2012). Geothermal resource characterization and evaluation at Astor Pass, Nevada. *Geothermal Resources Council Transactions*, 36, 1371-1376.
- Rybach, L. (2010). Status and prospects of geothermal energy. In Proc. World Geothermal Congress.
- Saltelli, A., Chan, K., & Scott, E. M. (Eds.). (2000). *Sensitivity Analysis*. New York: Wiley.
- Simunek, J., Van Genuchten, M. T., & Sejna, M. (2005). The HYDRUS-1D software package for simulating the one-dimensional movement of water, heat, and multiple solutes in variably-saturated media. *University of California-Riverside Research Reports*.
- Sladek, C., Coolbaugh, M. F., & Zehner, R. E. (2007). Development of 2-meter soil temperature probes and results of temperature survey conducted at Desert Peak, Nevada, USA. *Geothermal Resources Council Transactions*, 31, 363-368.
- Wood, J. R., and T. A. Hewett (1982). Fluid convection and mass transfer in porous limestones: A theoretical model. *Geochim. Cosmochim. Acta*, 46, 1707-1713.

**APPENDIX**  
**TOUGH2 Input Files**  
**Simulation 1 (Base Model)**

```

# run with eos3
ROCKS---1---*---2---*---3---*---4---*---5---*---6---*---7---*---8
sands  2    2000.    0.45  1.0e-11  1.0e-11  1.0e-11    2.0    830.
        1
        7        0.63    0.045    1.0    0.3
        7        0.63    0.04    1.48e-3    1.0e6    1.0
boun2  2    2000.    0.45  1.0e-14  1.0e-14  1.0e-14    2.0    1.e55
        1
        7        0.63    0.045    1.0    0.3
        7        0.63    0.04    1.48e-3    1.0e6    1.0
boun3  2    2000.    0.45  1.0e-25  1.0e-25  1.0e-25    2.0    1.e55
        1
        7        0.63    0.045    1.0    0.3
        7        0.63    0.04    1.48e-3    1.0e6    1.0

MULTI---1---*---2---*---3---*---4---*---5---*---6---*---7---*---8
      2  3  2  6
START---1---*---2---*---3---*---4---*---5---*---6---*---7---*---8
----*---1 MOP: 123456789*123456789*1234 ----*---5---*---6---*---7---*---8
PARAM---1---*---2---*---3---*---4---*---5---*---6---*---7---*---8
      8 29999 999100000100020001401000001
          0.  3.16e13    10.    A31 1    9.81
          1.e-5    1.    .1    1.    1.
          1.01e5    10.7    20.

SOLVR---1---*---2---*---3---*---4---*---5---*---6---*---7---*---8
      2  Z2  O0    1.0    1.e-6

TIMES---1---*---2---*---3---*---4---*---5---*---6---*---7---*---8
      4
      3.16e10  3.16e11  3.16e12  3.16e13
#INCON---1---*---2---*---3---*---4---*---5---*---6---*---7---*---8
#A11 1  24  1
#    1.01e5    10.9    20.
#AR1 1  24  1
#    1.01e5    1.0e-10    20.
#

ENDCY
MESHMAKER1---*---2---*---3---*---4---*---5---*---6---*---7---*---8
XYZ
      0.
NX  25    4.
NY  1    4.
NZ  1    1.e-6
NZ  25    4.
NZ  1    1.e-6

ENDFI

```

\* Note that input file for the large checkerboard and vertical layers model were the same and are referred to as heterogeneous.

## Simulation 2 (Homogeneous)

```

# run with eos3
ROCKS-----1-----*-----2-----*-----3-----*-----4-----*-----5-----*-----6-----*-----7-----*-----8
sands      2      2000.      0.45      1.0e-12      1.0e-12      1.0e-12      2.0      830.
           1
           7      0.63      0.045      1.0      0.3
           7      0.63      0.04      1.48e-3      1.0e6      1.0
boun2     2      2000.      0.45      1.0e-14      1.0e-14      1.0e-14      2.0      1.e55
           1
           7      0.63      0.045      1.0      0.3
           7      0.63      0.04      1.48e-3      1.0e6      1.0
boun3     2      2000.      0.45      0.0e-14      0.0e-14      0.0e-14      2.0      1.e55
           1
           7      0.63      0.045      1.0      0.3
           7      0.63      0.04      1.48e-3      1.0e6      1.0

MULTI-----1-----*-----2-----*-----3-----*-----4-----*-----5-----*-----6-----*-----7-----*-----8
  2      3      2      6
START-----1-----*-----2-----*-----3-----*-----4-----*-----5-----*-----6-----*-----7-----*-----8
-----*-----1 MOP: 123456789*123456789*1234 -----*-----5-----*-----6-----*-----7-----*-----8
PARAM-----1-----*-----2-----*-----3-----*-----4-----*-----5-----*-----6-----*-----7-----*-----8
  8 29999      999100000100020001401000001
           0.      3.16e13      10.      A31 1      9.81
           1.e-5      1.      .1      1.      1.
           1.01e5      10.7      20.
TIMES-----1-----*-----2-----*-----3-----*-----4-----*-----5-----*-----6-----*-----7-----*-----8
  1
  3.16e13
#INCON-----1-----*-----2-----*-----3-----*-----4-----*-----5-----*-----6-----*-----7-----*-----8
#A11 1 24 1
#      1.01e5      10.9      20.
#AR1 1 24 1
#      1.01e5      1.0e-10      20.
#

ENDCY
MESHMAKER1-----*-----2-----*-----3-----*-----4-----*-----5-----*-----6-----*-----7-----*-----8
XYZ
  0.
NX 25 4.
NY 1 4.
NZ 1 1.e-6
NZ 25 4.
NZ 1 1.e-6

ENDFI

```



### Simulations 10 & 18 (Heterogeneous)

```

# run with eos3
ROCKS-----1-----*-----2-----*-----3-----*-----4-----*-----5-----*-----6-----*-----7-----*-----8
sands      2      2000.      0.45  1.0e-11  1.0e-11  1.0e-11  2.0      830.
           1
           7      0.63      0.045  1.0      0.3
           7      0.63      0.04  1.48e-3  1.0e6  1.0
boun2     2      2000.      0.45  1.0e-12  1.0e-12  1.0e-12  2.0      830.
           1
           7      0.63      0.045  1.0      0.3
           7      0.63      0.04  1.48e-3  1.0e6  1.0
boun2     2      2000.      0.45  1.0e-14  1.0e-14  1.0e-14  2.0      1.e55
           1
           7      0.63      0.045  1.0      0.3
           7      0.63      0.04  1.48e-3  1.0e6  1.0
boun3     2      2000.      0.45  1.0e-25  1.0e-25  1.0e-25  2.0      1.e55
           1
           7      0.63      0.045  1.0      0.3
           7      0.63      0.04  1.48e-3  1.0e6  1.0

MULTI-----1-----*-----2-----*-----3-----*-----4-----*-----5-----*-----6-----*-----7-----*-----8
  2  3  2  6
START-----1-----*-----2-----*-----3-----*-----4-----*-----5-----*-----6-----*-----7-----*-----8
-----*-----1 MOP: 123456789*123456789*1234 -----*-----5-----*-----6-----*-----7-----*-----8
PARAM-----1-----*-----2-----*-----3-----*-----4-----*-----5-----*-----6-----*-----7-----*-----8
  8 29999      999100000100020001401000001
      0.  3.16e13      10.      A31 1      9.81
      1.e-5      1.      .1      1.      1.
      1.01e5      10.7      20.

SOLVR-----1-----*-----2-----*-----3-----*-----4-----*-----5-----*-----6-----*-----7-----*-----8
  2  Z2  00      1.0  1.e-6

TIMES-----1-----*-----2-----*-----3-----*-----4-----*-----5-----*-----6-----*-----7-----*-----8
  1
  3.16e10  3.16e11  3.16e12  3.16e13
#INCON-----1-----*-----2-----*-----3-----*-----4-----*-----5-----*-----6-----*-----7-----*-----8
#A11 1  24  1
# 1.01e5      10.9      20.
#AR1 1  24  1
# 1.01e5      1.0e-10      20.
#
#

ENDCY
MESHMAKER1-----*-----2-----*-----3-----*-----4-----*-----5-----*-----6-----*-----7-----*-----8
XYZ
  0.
NX  25  4.
NY  1  4.
NZ  1  1.e-6
NZ  25  4.
NZ  1  1.e-6

ENDFI

```

## Simulation 3 (Homogeneous)

```

# run with eos3
ROCKS-----1-----*-----2-----*-----3-----*-----4-----*-----5-----*-----6-----*-----7-----*-----8
sands      2      2000.      0.45      1.0e-10      1.0e-10      1.0e-10      2.0      830.
           1
           7      0.63      0.045      1.0      0.3
           7      0.63      0.04      1.48e-3      1.0e6      1.0
boun2      2      2000.      0.45      1.0e-14      1.0e-14      1.0e-14      2.0      1.e55
           1
           7      0.63      0.045      1.0      0.3
           7      0.63      0.04      1.48e-3      1.0e6      1.0
boun3      2      2000.      0.45      1.0e-25      1.0e-25      1.0e-25      2.0      1.e55
           1
           7      0.63      0.045      1.0      0.3
           7      0.63      0.04      1.48e-3      1.0e6      1.0

MULTI-----1-----*-----2-----*-----3-----*-----4-----*-----5-----*-----6-----*-----7-----*-----8
  2      3      2      6
START-----1-----*-----2-----*-----3-----*-----4-----*-----5-----*-----6-----*-----7-----*-----8
-----*-----1 MOP: 123456789*123456789*1234 -----*-----5-----*-----6-----*-----7-----*-----8
PARAM-----1-----*-----2-----*-----3-----*-----4-----*-----5-----*-----6-----*-----7-----*-----8
  8 29999      999100000100020001401000001
           0.      3.16e13      10.      A31 1      9.81
           1.e-5      1.      .1      1.      1.
           1.01e5      10.7      20.

SOLVR-----1-----*-----2-----*-----3-----*-----4-----*-----5-----*-----6-----*-----7-----*-----8
  2  Z2  00      1.0      1.e-6

TIMES-----1-----*-----2-----*-----3-----*-----4-----*-----5-----*-----6-----*-----7-----*-----8
  4
  3.16e10  3.16e11  3.16e12  3.16e13
#INCON-----1-----*-----2-----*-----3-----*-----4-----*-----5-----*-----6-----*-----7-----*-----8
#A11 1  24  1
#      1.01e5      10.9      20.
#AR1 1  24  1
#      1.01e5      1.0e-10      20.
#

ENDCY
MESHPAKER1-----*-----2-----*-----3-----*-----4-----*-----5-----*-----6-----*-----7-----*-----8
XYZ
  0.
NX  25      4.
NY  1      4.
NZ  1      1.e-6
NZ  25      4.
NZ  1      1.e-6

ENDFI

```

### Simulations 11 & 19 (Heterogeneous)

```

# run with eos3
ROCKS-----1-----*-----2-----*-----3-----*-----4-----*-----5-----*-----6-----*-----7-----*-----8
sands      2      2000.      0.45  1.0e-11  1.0e-11  1.0e-11      2.0      830.
           1
           7      0.63  0.045  1.0      0.3
           7      0.63  0.04  1.48e-3  1.0e6  1.0
boun2     2      2000.      0.45  1.0e-10  1.0e-10  1.0e-10      2.0      830.
           1
           7      0.63  0.045  1.0      0.3
           7      0.63  0.04  1.48e-3  1.0e6  1.0
boun2     2      2000.      0.45  1.0e-14  1.0e-14  1.0e-14      2.0      1.e55
           1
           7      0.63  0.045  1.0      0.3
           7      0.63  0.04  1.48e-3  1.0e6  1.0
boun3     2      2000.      0.45  1.0e-25  1.0e-25  1.0e-25      2.0      1.e55
           1
           7      0.63  0.045  1.0      0.3
           7      0.63  0.04  1.48e-3  1.0e6  1.0

MULTI-----1-----*-----2-----*-----3-----*-----4-----*-----5-----*-----6-----*-----7-----*-----8
  2  3  2  6
START-----1-----*-----2-----*-----3-----*-----4-----*-----5-----*-----6-----*-----7-----*-----8
-----*-----1 MOP: 123456789*123456789*1234 -----*-----5-----*-----6-----*-----7-----*-----8
PARAM-----1-----*-----2-----*-----3-----*-----4-----*-----5-----*-----6-----*-----7-----*-----8
  8 29999 999100000100020001401000001
      0.  3.16e13  10.  A31 1  9.81
      1.e-5  1.  .1  1.  1.
           1.01e5  10.7  20.

SOLVR-----1-----*-----2-----*-----3-----*-----4-----*-----5-----*-----6-----*-----7-----*-----8
  2  Z2  00  1.0  1.e-6

TIMES-----1-----*-----2-----*-----3-----*-----4-----*-----5-----*-----6-----*-----7-----*-----8
  4
  3.16e10  3.16e11  3.16e12  3.16e13
#INCON-----1-----*-----2-----*-----3-----*-----4-----*-----5-----*-----6-----*-----7-----*-----8
#A11 1  24  1
#  1.01e5  10.9  20.
#AR1 1  24  1
#  1.01e5  1.0e-10  20.
#

ENDCY
MESHMAKER1-----*-----2-----*-----3-----*-----4-----*-----5-----*-----6-----*-----7-----*-----8
XYZ
  0.
NX  25  4.
NY  1  4.
NZ  1  1.e-6
NX  25  4.
NZ  1  1.e-6

ENDFI

```

## Simulation 4 (Homogeneous)

```

# run with eos3
ROCKS-----1-----*-----2-----*-----3-----*-----4-----*-----5-----*-----6-----*-----7-----*-----8
sands      2      2000.      0.45      1.0e-11      1.0e-11      1.0e-11      0.5      830.
           1
           7      0.63      0.045      1.0      0.3
           7      0.63      0.04      1.48e-3      1.0e6      1.0
boun2     2      2000.      0.45      1.0e-14      1.0e-14      1.0e-14      2.0      1.e55
           1
           7      0.63      0.045      1.0      0.3
           7      0.63      0.04      1.48e-3      1.0e6      1.0
boun3     2      2000.      0.45      1.0e-25      1.0e-25      1.0e-25      2.0      1.e55
           1
           7      0.63      0.045      1.0      0.3
           7      0.63      0.04      1.48e-3      1.0e6      1.0

MULTI-----1-----*-----2-----*-----3-----*-----4-----*-----5-----*-----6-----*-----7-----*-----8
  2      3      2      6
START-----1-----*-----2-----*-----3-----*-----4-----*-----5-----*-----6-----*-----7-----*-----8
-----*-----1 MOP: 123456789*123456789*1234 -----*-----5-----*-----6-----*-----7-----*-----8
PARAM-----1-----*-----2-----*-----3-----*-----4-----*-----5-----*-----6-----*-----7-----*-----8
  8 29999      999100000100020001401000001
           0.      3.16e13      10.      A31 1      9.81
           1.e-5      1.      .1      1.      1.
           1.01e5      10.7      20.

SOLVR-----1-----*-----2-----*-----3-----*-----4-----*-----5-----*-----6-----*-----7-----*-----8
  2  Z2  00      1.0      1.e-6

TIMES-----1-----*-----2-----*-----3-----*-----4-----*-----5-----*-----6-----*-----7-----*-----8
  4
  3.16e10  3.16e11  3.16e12  3.16e13
#INCON-----1-----*-----2-----*-----3-----*-----4-----*-----5-----*-----6-----*-----7-----*-----8
#A11 1  24  1
#      1.01e5      10.9      20.
#AR1 1  24  1
#      1.01e5      1.0e-10      20.
#

ENDCY
MESHPAKER1-----*-----2-----*-----3-----*-----4-----*-----5-----*-----6-----*-----7-----*-----8
XYZ
  0.
NX  25      4.
NY  1      4.
NZ  1      1.e-6
NZ  25      4.
NZ  1      1.e-6

ENDFI

```

### Simulations 12 & 20 (Heterogeneous)

```

# run with eos3
ROCKS-----1-----*-----2-----*-----3-----*-----4-----*-----5-----*-----6-----*-----7-----*-----8
sands      2      2000.      0.45  1.0e-11  1.0e-11  1.0e-11  2.0      830.
           1
           7      0.63      0.045  1.0      0.3
           7      0.63      0.04  1.48e-3  1.0e6  1.0
boun2     2      2000.      0.45  1.0e-11  1.0e-11  1.0e-11  0.5      830.
           1
           7      0.63      0.045  1.0      0.3
           7      0.63      0.04  1.48e-3  1.0e6  1.0
boun2     2      2000.      0.45  1.0e-14  1.0e-14  1.0e-14  2.0      1.e55
           1
           7      0.63      0.045  1.0      0.3
           7      0.63      0.04  1.48e-3  1.0e6  1.0
boun3     2      2000.      0.45  1.0e-25  1.0e-25  1.0e-25  2.0      1.e55
           1
           7      0.63      0.045  1.0      0.3
           7      0.63      0.04  1.48e-3  1.0e6  1.0

MULTI-----1-----*-----2-----*-----3-----*-----4-----*-----5-----*-----6-----*-----7-----*-----8
      2      3      2      6
START-----1-----*-----2-----*-----3-----*-----4-----*-----5-----*-----6-----*-----7-----*-----8
-----*-----1 MOP: 123456789*123456789*1234 -----*-----5-----*-----6-----*-----7-----*-----8
PARAM-----1-----*-----2-----*-----3-----*-----4-----*-----5-----*-----6-----*-----7-----*-----8
      8 29999      999100000100020001401000001
           0.  3.16e13  10.  A31 1  9.81
           1.e-5  1.  .1  1.  1.
           1.01e5  10.7  20.

SOLVR-----1-----*-----2-----*-----3-----*-----4-----*-----5-----*-----6-----*-----7-----*-----8
      3  Z2  O0      1.0  1.e-6

TIMES-----1-----*-----2-----*-----3-----*-----4-----*-----5-----*-----6-----*-----7-----*-----8
      4
      3.16e10  3.16e11  3.16e12  3.16e13
#INCON-----1-----*-----2-----*-----3-----*-----4-----*-----5-----*-----6-----*-----7-----*-----8
#A11 1  24  1
#  1.01e5  10.9  20.
#AR1 1  24  1
#  1.01e5  1.0e-10  20.
#

ENDCY
MESHPMAKER1-----*-----2-----*-----3-----*-----4-----*-----5-----*-----6-----*-----7-----*-----8
XYZ
      0.
NX  25  4.
NY  1  4.
NZ  1  1.e-6
NZ  25  4.
NZ  1  1.e-6

ENDFI

```

## Simulation 5 (Homogeneous)

```

# run with eos3
ROCKS-----1-----*-----2-----*-----3-----*-----4-----*-----5-----*-----6-----*-----7-----*-----8
sands      2      2000.      0.45      1.0e-11      1.0e-11      1.0e-11      3.5      830.
           1
           7      0.63      0.045      1.0      0.3
           7      0.63      0.04      1.48e-3      1.0e6      1.0
boun2      2      2000.      0.45      1.0e-14      1.0e-14      1.0e-14      2.0      1.e55
           1
           7      0.63      0.045      1.0      0.3
           7      0.63      0.04      1.48e-3      1.0e6      1.0
boun3      2      2000.      0.45      1.0e-25      1.0e-25      1.0e-25      2.0      1.e55
           1
           7      0.63      0.045      1.0      0.3
           7      0.63      0.04      1.48e-3      1.0e6      1.0

MULTI-----1-----*-----2-----*-----3-----*-----4-----*-----5-----*-----6-----*-----7-----*-----8
      2      3      2      6
START-----1-----*-----2-----*-----3-----*-----4-----*-----5-----*-----6-----*-----7-----*-----8
-----*-----1 MOP: 123456789*123456789*1234 -----*-----5-----*-----6-----*-----7-----*-----8
PARAM-----1-----*-----2-----*-----3-----*-----4-----*-----5-----*-----6-----*-----7-----*-----8
      8 29999      999100000100020001401000001
           0.      3.16e13      10.      A31 1      9.81
           1.e-5      1.      .1      1.      1.
           1.01e5      10.7      20.

SOLVR-----1-----*-----2-----*-----3-----*-----4-----*-----5-----*-----6-----*-----7-----*-----8
      2      Z2      00      1.0      1.e-6

TIMES-----1-----*-----2-----*-----3-----*-----4-----*-----5-----*-----6-----*-----7-----*-----8
      4
           3.16e10      3.16e11      3.16e12      3.16e13
#INCON-----1-----*-----2-----*-----3-----*-----4-----*-----5-----*-----6-----*-----7-----*-----8
#A11 1      24      1
#      1.01e5      10.9      20.
#AR1 1      24      1
#      1.01e5      1.0e-10      20.
#

ENDCY
MESHPAKER1-----*-----2-----*-----3-----*-----4-----*-----5-----*-----6-----*-----7-----*-----8
XYZ
           0.
NX      25      4.
NY      1      4.
NZ      1      1.e-6
NZ      25      4.
NZ      1      1.e-6

ENDFI

```

### Simulations 13, 21, 26 & 27(Heterogeneous)

```

# run with eos3
ROCKS-----1-----*-----2-----*-----3-----*-----4-----*-----5-----*-----6-----*-----7-----*-----8
sands      2      2000.      0.45      1.0e-11      1.0e-11      1.0e-11      2.0      830.
           1
           7      0.63      0.045      1.0      0.3
           7      0.63      0.04      1.48e-3      1.0e6      1.0
boun2     2      2000.      0.45      1.0e-11      1.0e-11      1.0e-11      3.5      830.
           1
           7      0.63      0.045      1.0      0.3
           7      0.63      0.04      1.48e-3      1.0e6      1.0
boun2     2      2000.      0.45      1.0e-14      1.0e-14      1.0e-14      2.0      1.e55
           1
           7      0.63      0.045      1.0      0.3
           7      0.63      0.04      1.48e-3      1.0e6      1.0
boun3     2      2000.      0.45      1.0e-25      1.0e-25      1.0e-25      2.0      1.e55
           1
           7      0.63      0.045      1.0      0.3
           7      0.63      0.04      1.48e-3      1.0e6      1.0

MULTI-----1-----*-----2-----*-----3-----*-----4-----*-----5-----*-----6-----*-----7-----*-----8
  2      3      2      6
START-----1-----*-----2-----*-----3-----*-----4-----*-----5-----*-----6-----*-----7-----*-----8
-----*-----1 MOP: 123456789*123456789*1234 -----*-----5-----*-----6-----*-----7-----*-----8
PARAM-----1-----*-----2-----*-----3-----*-----4-----*-----5-----*-----6-----*-----7-----*-----8
  8 29999      999100000100020001401000001
      0.      3.16e13      10.      A31 1      9.81
      1.e-5      1.      .1      1.      1.
      1.01e5      10.7      20.

SOLVR-----1-----*-----2-----*-----3-----*-----4-----*-----5-----*-----6-----*-----7-----*-----8
  2  Z2  O0      1.0      1.e-6

TIMES-----1-----*-----2-----*-----3-----*-----4-----*-----5-----*-----6-----*-----7-----*-----8
  4
  3.16e10  3.16e11  3.16e12  3.16e13
#INCON-----1-----*-----2-----*-----3-----*-----4-----*-----5-----*-----6-----*-----7-----*-----8
#A11 1  24  1
#      1.01e5      10.9      20.
#AR1 1  24  1
#      1.01e5      1.0e-10      20.
#

ENDCY
MESHPMAKER1-----*-----2-----*-----3-----*-----4-----*-----5-----*-----6-----*-----7-----*-----8
XYZ
      0.
NX      25      4.
NY      1      4.
NZ      1      1.e-6
NZ      25      4.
NZ      1      1.e-6

ENDFI

```

## Simulation 6 (Homogeneous)

```

# run with eos3
ROCKS-----1-----*-----2-----*-----3-----*-----4-----*-----5-----*-----6-----*-----7-----*-----8
sands      2      2000.      0.25  1.0e-11  1.0e-11  1.0e-11  2.0      830.
           1
           7      0.63      0.045  1.0      0.3
           7      0.63      0.04  1.48e-3  1.0e6      1.0
boun2      2      2000.      0.45  1.0e-14  1.0e-14  1.0e-14  2.0      1.e55
           1
           7      0.63      0.045  1.0      0.3
           7      0.63      0.04  1.48e-3  1.0e6      1.0
boun3      2      2000.      0.45  1.0e-25  1.0e-25  1.0e-25  2.0      1.e55
           1
           7      0.63      0.045  1.0      0.3
           7      0.63      0.04  1.48e-3  1.0e6      1.0

MULTI-----1-----*-----2-----*-----3-----*-----4-----*-----5-----*-----6-----*-----7-----*-----8
  2      3      2      6
START-----1-----*-----2-----*-----3-----*-----4-----*-----5-----*-----6-----*-----7-----*-----8
-----*-----1 MOP: 123456789*123456789*1234 -----*-----5-----*-----6-----*-----7-----*-----8
PARAM-----1-----*-----2-----*-----3-----*-----4-----*-----5-----*-----6-----*-----7-----*-----8
  8 29999      999100000100020001401000001
           0.      3.16e13      10.      A31 1      9.81
           1.e-5      1.      .1      1.      1.
           1.01e5      10.7      20.

SOLVR-----1-----*-----2-----*-----3-----*-----4-----*-----5-----*-----6-----*-----7-----*-----8
  2  Z2  00      1.0      1.e-6

TIMES-----1-----*-----2-----*-----3-----*-----4-----*-----5-----*-----6-----*-----7-----*-----8
  4
  3.16e10  3.16e11  3.16e12  3.16e13
#INCON-----1-----*-----2-----*-----3-----*-----4-----*-----5-----*-----6-----*-----7-----*-----8
#A11 1  24  1
#      1.01e5      10.9      20.
#AR1 1  24  1
#      1.01e5      1.0e-10      20.
#

ENDCY
MESHPAKER1-----*-----2-----*-----3-----*-----4-----*-----5-----*-----6-----*-----7-----*-----8
XYZ
  0.
NX  25      4.
NY  1      4.
NZ  1      1.e-6
NZ  25      4.
NZ  1      1.e-6

ENDFI

```



### Simulations 14 & 22 (Heterogeneous)

```

# run with eos3
ROCKS-----1-----*-----2-----*-----3-----*-----4-----*-----5-----*-----6-----*-----7-----*-----8
sands      2      2000.      0.45  1.0e-11  1.0e-11  1.0e-11  2.0      830.
           1
           7      0.63      0.045  1.0      0.3
           7      0.63      0.04  1.48e-3  1.0e6  1.0
boun2     2      2000.      0.25  1.0e-11  1.0e-11  1.0e-11  2.0      830.
           1
           7      0.63      0.045  1.0      0.3
           7      0.63      0.04  1.48e-3  1.0e6  1.0
boun2     2      2000.      0.45  1.0e-14  1.0e-14  1.0e-14  2.0      1.e55
           1
           7      0.63      0.045  1.0      0.3
           7      0.63      0.04  1.48e-3  1.0e6  1.0
boun3     2      2000.      0.45  1.0e-25  1.0e-25  1.0e-25  2.0      1.e55
           1
           7      0.63      0.045  1.0      0.3
           7      0.63      0.04  1.48e-3  1.0e6  1.0

MULTI-----1-----*-----2-----*-----3-----*-----4-----*-----5-----*-----6-----*-----7-----*-----8
  2      3      2      6
START-----1-----*-----2-----*-----3-----*-----4-----*-----5-----*-----6-----*-----7-----*-----8
-----*-----1 MOP: 123456789*123456789*1234 -----*-----5-----*-----6-----*-----7-----*-----8
PARAM-----1-----*-----2-----*-----3-----*-----4-----*-----5-----*-----6-----*-----7-----*-----8
  8 29999      999100000100020001401000001
      0.      3.16e13      10.      A31 1      9.81
      1.e-5      1.      .1      1.      1.
      1.01e5      10.7      20.

SOLVR-----1-----*-----2-----*-----3-----*-----4-----*-----5-----*-----6-----*-----7-----*-----8
  2  Z2  O0      1.0      1.e-6

TIMES-----1-----*-----2-----*-----3-----*-----4-----*-----5-----*-----6-----*-----7-----*-----8
  4
  3.16e10  3.16e11  3.16e12  3.16e13
#INCON-----1-----*-----2-----*-----3-----*-----4-----*-----5-----*-----6-----*-----7-----*-----8
#A11 1  24  1
#      1.01e5      10.9      20.
#AR1 1  24  1
#      1.01e5      1.0e-10      20.
#

ENDCY
MESHPMAKER1-----*-----2-----*-----3-----*-----4-----*-----5-----*-----6-----*-----7-----*-----8
XYZ
  0.
NX  25      4.
NY  1      4.
NZ  1      1.e-6
NZ  25      4.
NZ  1      1.e-6

ENDFI

```

## Simulation 7 (Homogeneous)

```

# run with eos3
ROCKS-----1-----*-----2-----*-----3-----*-----4-----*-----5-----*-----6-----*-----7-----*-----8
sands      2      2000.      0.50      1.0e-11      1.0e-11      1.0e-11      2.0      830.
           1
           7      0.63      0.045      1.0      0.3
           7      0.63      0.04      1.48e-3      1.0e6      1.0
boun2      2      2000.      0.45      1.0e-14      1.0e-14      1.0e-14      2.0      1.e55
           1
           7      0.63      0.045      1.0      0.3
           7      0.63      0.04      1.48e-3      1.0e6      1.0
boun3      2      2000.      0.45      1.0e-25      1.0e-25      1.0e-25      2.0      1.e55
           1
           7      0.63      0.045      1.0      0.3
           7      0.63      0.04      1.48e-3      1.0e6      1.0

MULTI-----1-----*-----2-----*-----3-----*-----4-----*-----5-----*-----6-----*-----7-----*-----8
  2      3      2      6
START-----1-----*-----2-----*-----3-----*-----4-----*-----5-----*-----6-----*-----7-----*-----8
-----*-----1 MOP: 123456789*123456789*1234 -----*-----5-----*-----6-----*-----7-----*-----8
PARAM-----1-----*-----2-----*-----3-----*-----4-----*-----5-----*-----6-----*-----7-----*-----8
  8 29999      999100000100020001401000001
           0.      3.16e13      10.      A31 1      9.81
           1.e-5      1.      .1      1.      1.
           1.01e5      10.7      20.

SOLVR-----1-----*-----2-----*-----3-----*-----4-----*-----5-----*-----6-----*-----7-----*-----8
  2  Z2  00      1.0      1.e-6

TIMES-----1-----*-----2-----*-----3-----*-----4-----*-----5-----*-----6-----*-----7-----*-----8
  4
  3.16e10  3.16e11  3.16e12  3.16e13
#INCON-----1-----*-----2-----*-----3-----*-----4-----*-----5-----*-----6-----*-----7-----*-----8
#A11 1  24  1
#      1.01e5      10.9      20.
#AR1 1  24  1
#      1.01e5      1.0e-10      20.
#

ENDCY
MESHPAKER1-----*-----2-----*-----3-----*-----4-----*-----5-----*-----6-----*-----7-----*-----8
XYZ
  0.
NX  25      4.
NY  1      4.
NZ  1      1.e-6
NZ  25      4.
NZ  1      1.e-6

ENDFI

```

### Simulations 15 & 23 (Heterogeneous)

```

# run with eos3
ROCKS-----1-----*-----2-----*-----3-----*-----4-----*-----5-----*-----6-----*-----7-----*-----8
sands      2      2000.      0.45  1.0e-11  1.0e-11  1.0e-11  2.0      830.
           1
           7      0.63      0.045  1.0      0.3
           7      0.63      0.04  1.48e-3  1.0e6      1.0
boun2     2      2000.      0.50  1.0e-11  1.0e-11  1.0e-11  2.0      830.
           1
           7      0.63      0.045  1.0      0.3
           7      0.63      0.04  1.48e-3  1.0e6      1.0
boun2     2      2000.      0.45  1.0e-14  1.0e-14  1.0e-14  2.0      1.e55
           1
           7      0.63      0.045  1.0      0.3
           7      0.63      0.04  1.48e-3  1.0e6      1.0
boun3     2      2000.      0.45  1.0e-25  1.0e-25  1.0e-25  2.0      1.e55
           1
           7      0.63      0.045  1.0      0.3
           7      0.63      0.04  1.48e-3  1.0e6      1.0

MULTI-----1-----*-----2-----*-----3-----*-----4-----*-----5-----*-----6-----*-----7-----*-----8
  2      3      2      6
START-----1-----*-----2-----*-----3-----*-----4-----*-----5-----*-----6-----*-----7-----*-----8
-----*-----1 MOP: 123456789*123456789*1234 ---*-----5-----*-----6-----*-----7-----*-----8
PARAM-----1-----*-----2-----*-----3-----*-----4-----*-----5-----*-----6-----*-----7-----*-----8
  8 29999      999100000100020001401000001
           0.  3.16e13      10.      A31 1      9.81
           1.e-5      1.      .1      1.      1.
           1.01e5      10.7      20.

SOLVR-----1-----*-----2-----*-----3-----*-----4-----*-----5-----*-----6-----*-----7-----*-----8
  3 Z2  00      1.0      1.e-6

TIMES-----1-----*-----2-----*-----3-----*-----4-----*-----5-----*-----6-----*-----7-----*-----8
  4
  3.16e10  3.16e11  3.16e12  3.16e13
#INCON-----1-----*-----2-----*-----3-----*-----4-----*-----5-----*-----6-----*-----7-----*-----8
#A11 1  24      1
#      1.01e5      10.9      20.
#AR1 1  24      1
#      1.01e5      1.0e-10      20.
#

ENDCY
MESHMAKER1-----*-----2-----*-----3-----*-----4-----*-----5-----*-----6-----*-----7-----*-----8
XYZ
  0.
NX      25      4.
NY      1      4.
NZ      1      1.e-6
NZ      25      4.
NZ      1      1.e-6

ENDFI

```

## Simulation 8 (Homogeneous)

```

# run with eos3
ROCKS-----1-----*-----2-----*-----3-----*-----4-----*-----5-----*-----6-----*-----7-----*-----8
sands      2      2000.      0.45      1.0e-11      1.0e-11      1.0e-11      2.0      830.
           1
           7      0.63      0.10      1.0      0.3
           7      0.63      0.075     1.48e-3     1.0e6      1.0
boun2      2      2000.      0.45      1.0e-14     1.0e-14     1.0e-14     2.0      1.e55
           1
           7      0.63      0.045     1.0      0.3
           7      0.63      0.04      1.48e-3     1.0e6      1.0
boun3      2      2000.      0.45      1.0e-25     1.0e-25     1.0e-25     2.0      1.e55
           1
           7      0.63      0.045     1.0      0.3
           7      0.63      0.04      1.48e-3     1.0e6      1.0

MULTI-----1-----*-----2-----*-----3-----*-----4-----*-----5-----*-----6-----*-----7-----*-----8
  2      3      2      6
START-----1-----*-----2-----*-----3-----*-----4-----*-----5-----*-----6-----*-----7-----*-----8
-----*-----1 MOP: 123456789*123456789*1234 -----*-----5-----*-----6-----*-----7-----*-----8
PARAM-----1-----*-----2-----*-----3-----*-----4-----*-----5-----*-----6-----*-----7-----*-----8
  8 29999      999100000100020001401000001
           0.      3.16e13      10.      A31 1      9.81
           1.e-5      1.      .1      1.      1.
           1.01e5      10.7      20.

SOLVR-----1-----*-----2-----*-----3-----*-----4-----*-----5-----*-----6-----*-----7-----*-----8
  2  Z2  00      1.0      1.e-6

TIMES-----1-----*-----2-----*-----3-----*-----4-----*-----5-----*-----6-----*-----7-----*-----8
  4
  3.16e10  3.16e11  3.16e12  3.16e13
#INCON-----1-----*-----2-----*-----3-----*-----4-----*-----5-----*-----6-----*-----7-----*-----8
#A11 1  24  1
#      1.01e5      10.9      20.
#AR1 1  24  1
#      1.01e5      1.0e-10      20.
#

ENDCY
MESHPAKER1-----*-----2-----*-----3-----*-----4-----*-----5-----*-----6-----*-----7-----*-----8
XYZ
  0.
NX  25      4.
NY  1      4.
NZ  1      1.e-6
NZ  25      4.
NZ  1      1.e-6

ENDFI

```

### Simulations 16 & 24 (Heterogeneous)

```

# run with eos3
ROCKS-----1-----*-----2-----*-----3-----*-----4-----*-----5-----*-----6-----*-----7-----*-----8
sands      2      2000.      0.45  1.0e-11  1.0e-11  1.0e-11      2.0      830.
           1
           7      0.63      0.045  1.0      0.3
           7      0.63      0.04  1.48e-3  1.0e6      1.0
boun2     2      2000.      0.45  1.0e-11  1.0e-11  1.0e-11      2.0      830.
           1
           7      0.63      0.1      1.0      0.3
           7      0.63      0.095  1.48e-3  1.0e6      1.0
boun2     2      2000.      0.45  1.0e-14  1.0e-14  1.0e-14      2.0      1.e55
           1
           7      0.63      0.045  1.0      0.3
           7      0.63      0.04  1.48e-3  1.0e6      1.0
boun3     2      2000.      0.45  1.0e-25  1.0e-25  1.0e-25      2.0      1.e55
           1
           7      0.63      0.045  1.0      0.3
           7      0.63      0.04  1.48e-3  1.0e6      1.0

MULTI-----1-----*-----2-----*-----3-----*-----4-----*-----5-----*-----6-----*-----7-----*-----8
  2  3  2  6
START-----1-----*-----2-----*-----3-----*-----4-----*-----5-----*-----6-----*-----7-----*-----8
-----*-----1 MOP: 123456789*123456789*1234 -----*-----5-----*-----6-----*-----7-----*-----8
PARAM-----1-----*-----2-----*-----3-----*-----4-----*-----5-----*-----6-----*-----7-----*-----8
  8 29999 999100000100020001401000001
      0.  3.16e13  10.  A31 1 9.81
      1.e-5 1. .1 1. 1.
           1.01e5 10.7 20.

SOLVR-----1-----*-----2-----*-----3-----*-----4-----*-----5-----*-----6-----*-----7-----*-----8
  2  Z2  O0  1.0  1.e-6

TIMES-----1-----*-----2-----*-----3-----*-----4-----*-----5-----*-----6-----*-----7-----*-----8
  4
  3.16e10 3.16e11 3.16e12 3.16e13
#INCON-----1-----*-----2-----*-----3-----*-----4-----*-----5-----*-----6-----*-----7-----*-----8
#A11 1 24 1
# 1.01e5 10.9 20.
#AR1 1 24 1
# 1.01e5 1.0e-10 20.
#

ENDCY
MESHMAKER1-----*-----2-----*-----3-----*-----4-----*-----5-----*-----6-----*-----7-----*-----8
XYZ
  0.
NX 25 4.
NY 1 4.
NZ 1 1.e-6
NZ 25 4.
NZ 1 1.e-6

ENDFI

```

## Simulation 9 (Homogeneous)

```

# run with eos3
ROCKS---1---*---2---*---3---*---4---*---5---*---6---*---7---*---8
sands  2    2000.    0.45  1.0e-11  1.0e-11  1.0e-11  2.0    830.
        1
        7    0.63    0.15    1.0    0.3
        7    0.63    0.125  1.48e-3  1.0e6    1.0
boun2  2    2000.    0.45  1.0e-14  1.0e-14  1.0e-14  2.0    1.e55
        1
        7    0.63    0.045   1.0    0.3
        7    0.63    0.04   1.48e-3  1.0e6    1.0
boun3  2    2000.    0.45  1.0e-25  1.0e-25  1.0e-25  2.0    1.e55
        1
        7    0.63    0.045   1.0    0.3
        7    0.63    0.04   1.48e-3  1.0e6    1.0

MULTI---1---*---2---*---3---*---4---*---5---*---6---*---7---*---8
      2  3  2  6
START---1---*---2---*---3---*---4---*---5---*---6---*---7---*---8
-----*---1 MOP: 123456789*123456789*1234 -----*---5---*---6---*---7---*---8
PARAM---1---*---2---*---3---*---4---*---5---*---6---*---7---*---8
      8 29999 999100000100020001401000001
          0.  3.16e13  10.  A31 1  9.81
          1.e-5  1.  .1  1.  1.
          1.01e5  10.7  20.

SOLVR---1---*---2---*---3---*---4---*---5---*---6---*---7---*---8
      2  Z2  00  1.0  1.e-6

TIMES---1---*---2---*---3---*---4---*---5---*---6---*---7---*---8
      4
      3.16e10  3.16e11  3.16e12  3.16e13
#INCON---1---*---2---*---3---*---4---*---5---*---6---*---7---*---8
#A11 1  24  1
#  1.01e5  10.9  20.
#AR1 1  24  1
#  1.01e5  1.0e-10  20.
#

ENDCY
MESHPAKER1---*---2---*---3---*---4---*---5---*---6---*---7---*---8
XYZ
      0.
NX  25  4.
NY  1  4.
NZ  1  1.e-6
NZ  25  4.
NZ  1  1.e-6

ENDFI

```

### Simulations 17 & 25 (Heterogeneous)

```

# run with eos3
ROCKS-----1-----*-----2-----*-----3-----*-----4-----*-----5-----*-----6-----*-----7-----*-----8
sands      2      2000.      0.45  1.0e-11  1.0e-11  1.0e-11  2.0      830.
           1
           7      0.63      0.045  1.0      0.3
           7      0.63      0.04  1.48e-3  1.0e6      1.0
boun2     2      2000.      0.45  1.0e-11  1.0e-11  1.0e-11  2.0      830.
           1
           7      0.63      0.15      1.0      0.3
           7      0.63      0.145  1.48e-3  1.0e6      1.0
boun2     2      2000.      0.45  1.0e-14  1.0e-14  1.0e-14  2.0      1.e55
           1
           7      0.63      0.045  1.0      0.3
           7      0.63      0.04  1.48e-3  1.0e6      1.0
boun3     2      2000.      0.45  1.0e-25  1.0e-25  1.0e-25  2.0      1.e55
           1
           7      0.63      0.045  1.0      0.3
           7      0.63      0.04  1.48e-3  1.0e6      1.0

MULTI-----1-----*-----2-----*-----3-----*-----4-----*-----5-----*-----6-----*-----7-----*-----8
  2      3      2      6
START-----1-----*-----2-----*-----3-----*-----4-----*-----5-----*-----6-----*-----7-----*-----8
-----*-----1 MOP: 123456789*123456789*1234 -----*-----5-----*-----6-----*-----7-----*-----8
PARAM-----1-----*-----2-----*-----3-----*-----4-----*-----5-----*-----6-----*-----7-----*-----8
  8 29999      999100000100020001401000001
      0.      3.16e13      10.      A31 1      9.81
      1.e-5      1.      .1      1.      1.
      1.01e5      10.7      20.

SOLVR-----1-----*-----2-----*-----3-----*-----4-----*-----5-----*-----6-----*-----7-----*-----8
  3  Z2  O0      1.0      1.e-6

TIMES-----1-----*-----2-----*-----3-----*-----4-----*-----5-----*-----6-----*-----7-----*-----8
  4
  3.16e10  3.16e11  3.16e12  3.16e13
#INCON-----1-----*-----2-----*-----3-----*-----4-----*-----5-----*-----6-----*-----7-----*-----8
#A11 1  24  1
#      1.01e5      10.9      20.
#AR1 1  24  1
#      1.01e5      1.0e-10      20.
#

ENDCY
MESHPMAKER1-----*-----2-----*-----3-----*-----4-----*-----5-----*-----6-----*-----7-----*-----8
XYZ
  0.
NX  25      4.
NY  1      4.
NZ  1      1.e-6
NZ  25      4.
NZ  1      1.e-6

ENDFI

```